Late Pleistocene and Holocene uplift history of Cyprus: implications for active tectonics along the southern margin of the Anatolian microplate

Article *in* Geological Society London Special Publications · July 2013

DOI: 10.1144/SP372.3

CITATIONS
18

READS
371

7 authors, including:

Efthymios Tsiolakis
Ministry of Agriculture, Natural Resources and Environment
10 PUBLICATIONS **135** CITATIONS
SEE PROFILE

Byron Stone
United States Geological Survey
28 PUBLICATIONS **251** CITATIONS
SEE PROFILE

Alan R. Lord
Senckenberg Research Institute
87 PUBLICATIONS **1,629** CITATIONS
SEE PROFILE

Shannon A Mahan
United States Geological Survey
235 PUBLICATIONS **2,203** CITATIONS
SEE PROFILE

Geological Society, London, Special Publications

Late Pleistocene and Holocene uplift history of Cyprus: implications for active tectonics along the southern margin of the Anatolian microplate

R. W. Harrison, E. Tsiolakis, B. D. Stone, A. Lord, J. P. McGeehin, S. A. Mahan and P. Chirico

Geological Society, London, Special Publications 2013, v.372; p561-584.
doi: 10.1144/SP372.3

Notes

Late Pleistocene and Holocene uplift history of Cyprus: implications for active tectonics along the southern margin of the Anatolian microplate

R. W. HARRISON[1]*, E. TSIOLAKIS[2], B. D. STONE[1], A. LORD[3], J. P. MCGEEHIN[1], S. A. MAHAN[4] & P. CHIRICO[1]

[1]*US Geological Survey, MS926A National Center, Reston, VA 20192, USA*

[2]*Geological Survey Department of Cyprus, Lefkosia 1415, Cyprus*

[3]*Senckenberg Forschungsinstitut und Naturmuseum, Senckenberganlage 25, D-60325 Frankfurt-am-Main, Germany*

[4]*US Geological Survey, Denver Federal Center, Box 25046, MS 974, Denver, CO 80225-0046, USA*

**Corresponding author (e-mail: rharriso@usgs.gov)*

Abstract: The nature of the southern margin of the Anatolian microplate during the Neogene is complex, controversial and fundamental in understanding active plate-margin tectonics and natural hazards in the Eastern Mediterranean region. Our investigation provides new insights into the Late Pleistocene uplift history of Cyprus and the Troodos Ophiolite. We provide isotopic (^{14}C) and radiogenic (luminescence) dates of outcropping marine sediments in eastern Cyprus that identify periods of deposition during marine isotope stages (MIS) 3, 4, 5 and 6. Past sea-levels indicated by these deposits are *c.* 95 $\pm$ 25 m higher in elevation than estimates of worldwide eustatic sea-level. An uplift rate of *c.* 1.8 mm/year and possibly as much as *c.* 4.1 mm/year in the past *c.* 26–40 ka is indicated. Holocene marine deposits also occur at elevations higher than those expected for past SL and suggest uplift rates of *c.* 1.2–2.1 mm/year. MIS-3 marine deposits that crop out in southern and western Cyprus indicate uniform island-wide uplift. We propose a model of tectonic wedging at a plate-bounding restraining bend as a mechanism for Late Pleistocene to Holocene uplift of Cyprus; uplift is accommodated by deformation and seismicity along the margins of the Troodos Ophiolite and re-activation of its low-angle, basal shear zone.

Supplementary material: An expanded description of the procedures used in determining OSL ages for samples given in Table 2 is available at www.geolsoc.org.uk/SUP18533.

The Eastern Mediterranean region has had a complex tectonic history since the Early Mesozoic breakup of Gondwana. Between the major plates of Africa and Eurasia, there is a >1500 km-wide intervening collage of differing tectonic terranes that is the product of shearing, rifting, subduction, obduction and contraction over the past 200 Ma. The dynamics of plate interactions and diastrophism, both past and present, are recorded in the assembly of this collage.

The island of Cyprus is in the middle of Neogene tectonic interaction between the Anatolian microplate on the southern margin of the Eurasian plate and fragmented blocks (Sinai block, Nubian microplate) of the African plate (Fig. 1). Structures off the southern coast of Cyprus are widely considered as accommodating both convergence and left-lateral strike-slip motion between these plates (McKenzie, 1970; Dewey *et al.* 1973; Robertson *et al.* 1995; Garfunkel 1998; Pinar & Kalafat 1999; Makris *et al.* 2000; Vidal *et al.* 2000; Harrison *et al.* 2004, 2008; Schattner, 2010). However, most individual aspects of the tectonic setting are controversial, as there exist many varying hypotheses and interpretations. For example, there are two competing hypotheses on the nature of major structures off the south coast of Cyprus in the respective roles of subduction v. transform faulting. These are: (1) that a northerly dipping subduction zone, which has consumed oceanic crust since the Late Cretaceous, exists south of Cyprus (Woodside 1977; Poole & Robertson 1991; Robertson *et al.* 1995; Robertson 2000; Schattner 2010) and (2) that multiple left-lateral transform systems intersect south of Cyprus that help accommodate regional escape tectonics (Neev 1977; Kemplar & Garfunkel 1994; Makris *et al.* 2000; Harrison & Panayides 2004; Harrison *et al.* 2004, 2008).

It is our opinion that, in the absence of a volcanic arc that can be linked to a subsiding oceanic slab

From: Robertson, A. H. F., Parlak, O. & Ünlügenç, U. C. (eds) 2013. *Geological Development of Anatolia and the Easternmost Mediterranean Region*. Geological Society, London, Special Publications, **372**, 561–584.
First published online August 22, 2012, http://dx.doi.org/10.1144/SP372.3

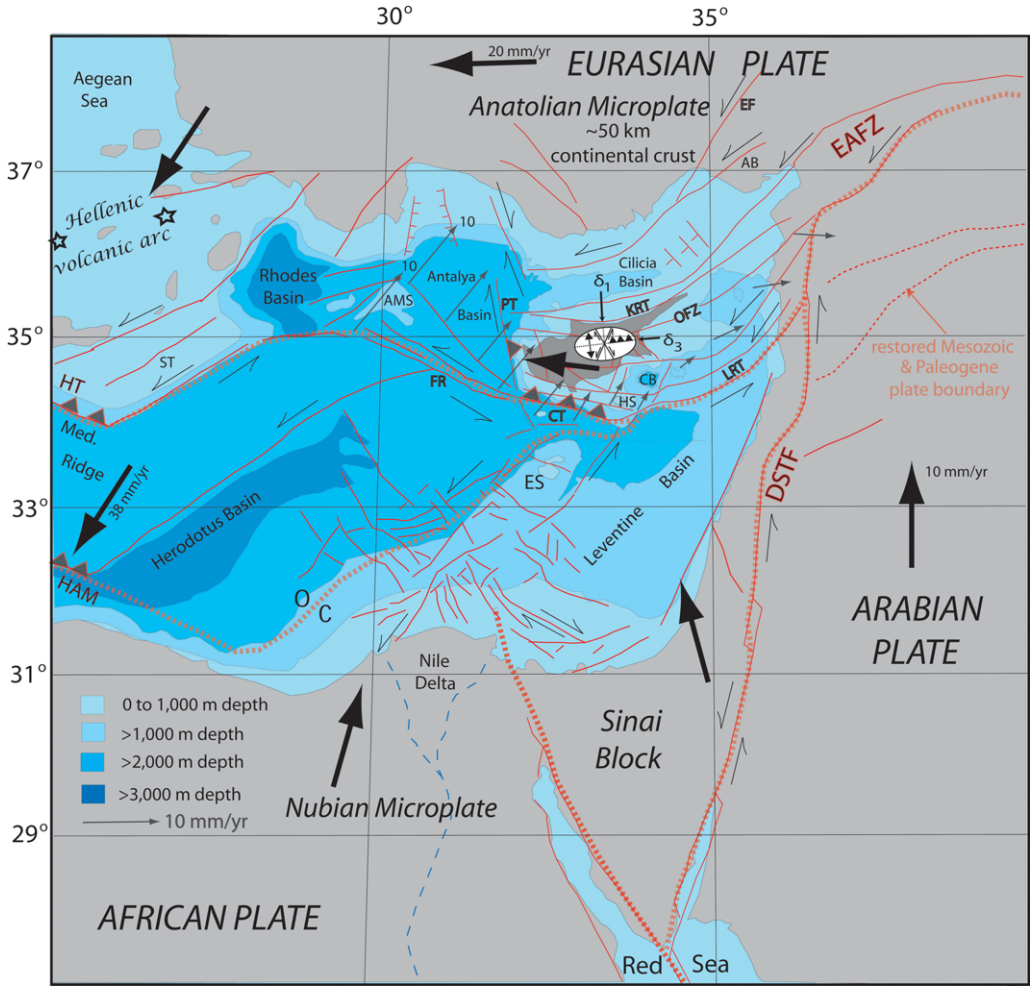

Fig. 1. Tectonic map of major crustal features between the Eurasian and African plates in the Eastern Mediterranean region, modified and adapted after Harrison *et al.* (2004, 2008) and many others sources, including Vidal *et al.* (2000), ten Veen *et al.* (2004), Neev (1977), Papazachos & Papaioannou (1999), Robertson (2000), Aal *et al.* (2001), Kemplar & Garfunkel (1994). Cyprus is shaded and is the only island in the eastern Mediterranean Sea. ES, Eratosthenes Seamount; CB, Cyprus Basin; FR, Florence Ridge fault zone; HS, Herodotus Seamount; AB, Adana Basin; ST, Strabo Trench; AMS, Anaximander Mts Seamount; EF, Ecemiş Fault; EAFZ, Eastern Anatolian fault zone (approximate palaeolocation restored to Mesozoic and Palaeogene time shown); DSTF, Dead Sea transform fault; HT, Hellenic trench; HAM, active Hellenic margin; PT, Polis transform fault zone; CT, Cyprus transform fault zone; LRT, Larnaca Ridge transform fault zone; KRT, Kyrenia Range thrust system; OFZ, Ovgos fault zone. Cyprus strain ellipse and orientations of maximum and minimum horizontal stresses ($\delta 1$ and $\delta 3$) are from Harrison *et al.* (2004, 2008). Approximate boundary between oceanic and continental crust south of Cyprus from Aal *et al.* (2001) is indicated by O and C; large arrows represent relative plate motions after Jackson and McKenzie (1988) and McClusky *et al.* (2000). The fault system between Cyprus and ES is the Cypriot transform, which marks the southern Anatolian microplate boundary. Bold dashed red lines are major crustal boundaries; thin red lines are regional faults; black half arrows show relative horizontal motion along faults. Thin shaded full arrows portray relative motion between the Anatolian microplate and African plate after Wdowinski *et al.* (2006).

beneath Cyprus, any post-Miocene subduction-zone model for Cyprus is disfavoured. Our alternative model is that today's active tectonic setting is one of strike-slip (transform) tectonics that has dominated the region since the Oligocene opening of the Gulf-of-Suez rift and subsequent Early to Middle Miocene Red Sea spreading and development of the Dead Sea transform (Mahmoud *et al.*

2005). This coincided with the northward translation of the Arabian plate and its impingement into the Eurasian plate as an indenter, which drives the western escape of the Anatolian microplate (Şengör *et al.* 1985; Burke & Şengör 1986), similar to a lemon seed being squeezed between two fingers. Burke and Şengör (1986) used the term 'scholle' for crustal fragments that are expelled sideways between strike-slip faults with opposite directions of motion towards areas of overthrusting in continent–continent collisions and subduction in continent–oceanic settings. In this aspect, Anatolia is a scholle that is moving westward between the right-lateral North Anatolia fault zone and several left-lateral fault zones on its southern margin, including the East Anatolia fault zone and the Cyprus transform of Harrison *et al.* (2004, 2008), which is otherwise known as the Cyprus arc. Cyprus is moving with Anatolia (Fig. 1), and similar to the seed analogy, the maximum stress (δ^1) on Cyprus is horizontal and oriented orthogonal to the island's western motion, illustrated by the stress–strain ellipse in Figure 1. Our working hypothesis is that transform structures accommodate the westward escape of Anatolia and Cyprus. Crustal uplift occurs at restraining bends and subsidence at releasing bends (see Bridwell 1975; Mann 2007; Swanson 2005) formed by fault curvature and by strain transfer between parallel strike-slip structures along the plate boundary south of Cyprus (Harrison *et al.* 2004, 2008).

One aspect of active tectonics that can be studied and evaluated to better understand lithospheric activity in the Eastern Mediterranean region is crustal uplift. Sediments on Cyprus provide relatively easy access to information on the uplift history of this island. Following is a description of the stratigraphy found on the Larnaca Lowlands shelf and eastern Mesaoria Basin and information contained within the section that is relative to past eustatic sea-level (SL). We then compare past SL determined for Cyprus with worldwide estimates of previous SL in order to interpret the uplift history of the southeastern portion of the island from the last interglacial period to the Present. All of our references to past SL are based on the mean values of Siddall *et al.* (2003) for the Red Sea and Shackleton *et al.* (2000) for the Iberian margin.

Late Pleistocene and Holocene Marine stratigraphy of the Larnaca Lowlands shelf and eastern Mesaoria Basin

The Larnaca Lowlands shelf is a gently seaward-dipping platform that extends from the bedrock uplands of the Troodos Mountains, *c.* 4–6 km inland from the coast, to *c.* 4–6 km offshore, where there is a precipitous drop in the bathymetry into the Cyprus Basin (Figs 2 & 3). The slope of the shelf is about 7.0–7.5 m/km or $<0.5^{\circ}$. The emerged portion of the shelf is called the Larnaca Lowlands. Substrata that form the floor of the shelf are composed of marl and sandy marl of the Nicosia Formation (latest Miocene to Early Pleistocene), gypsum and marl of the Kalavasos Formation (Messinian), and chalk of the Pakhna Formation (Miocene). The floor of the shelf is an erosional surface that was cut into substrata at some unknown time in the Early to Middle Pleistocene. Substrata crop out locally, but much of the Larnaca Lowlands is covered by the Late Pleistocene and Holocene alluvial fan and marine deposits, the latter of which crop out in a 1–3 km-wide belt from Cape Kiti northward through the city of Larnaca (Fig. 4). Typically, Late Pleistocene marine deposits form ridges and hills that are as much as 30 m in elevation and lie unconformably upon substrata, and Holocene marine deposits crop out from 0 to 3 m above SL. A palaeo-estuary (shown on Figs 3 & 4) that is cut into substrata exists along a system of faults of Late Pleistocene and Holocene age (Larnaca fault zone of Harrison & Tsiolakis 2007). The palaeo-estuary is now occupied by salt lakes, whose surfaces are below SL and are underlain by Holocene marine deposits. Alluvial fan deposits overlie and fill broad channels cut into the Late Pleistocene marine deposits.

Previous work in the Larnaca Lowlands and eastern Mesaoria Basin

In a study of the Larnaca Lowlands by Bagnall (1960), the entire Quaternary marine section was grouped together and called the 'Shelly Sandstones' of Pleistocene age. Bagnall (1960) recognized that a sandy conglomerate typically occurred at the base of the section and that these deposits had accumulated in a shallow-water marine environment 'at no great distance from a shore line and conditions were probably very similar to those observed on the beaches of Cyprus at the present time'. Bagnall (1960) considered the alluvial fan deposits in the lowlands as the oldest Pleistocene unit. Gifford (1978) developed a geochronology for the Holocene marine deposits along the coast and within the salt lakes, as part of a palaeogeographic study of archaeological sites in the Larnaca Lowlands; his data are included in Table 1. Morhange *et al.* (2000) further expanded the Holocene geochronology for marine deposits around the archaeological site of Kition, a Late Bronze Age city near the heart of present-day Larnaca, and its ancient port of Bamboula; their data also are included in Table 1.

Poole *et al.* (1990) and Poole and Robertson (1991) viewed the Pleistocene marine section as consisting of multiple terrace levels that were

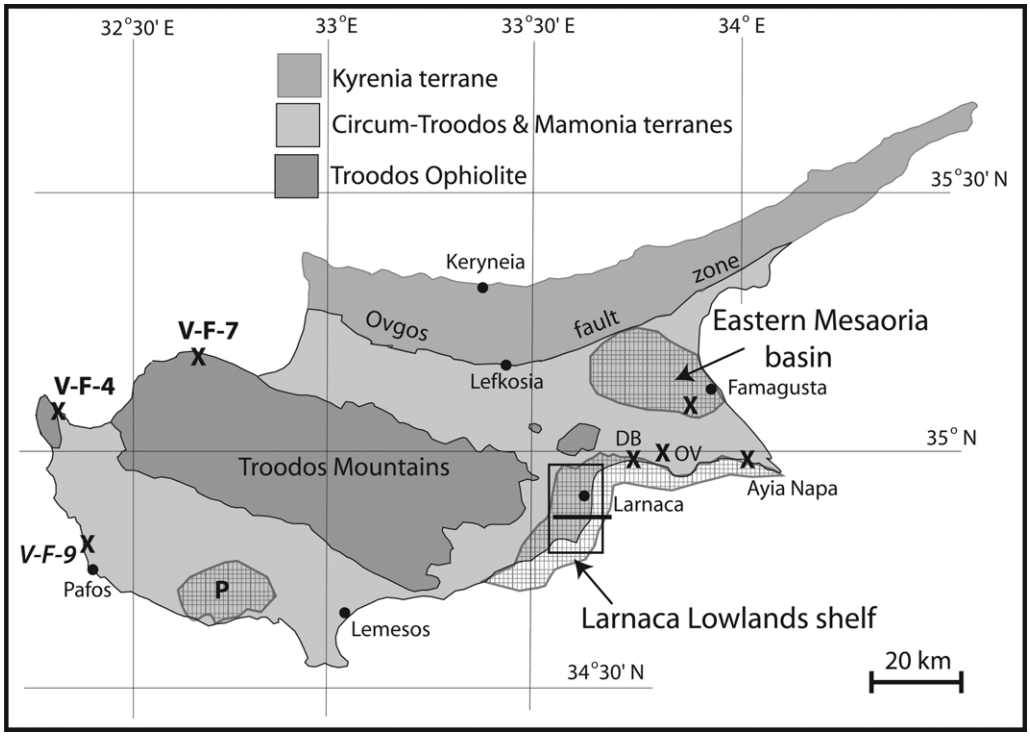

Fig. 2. Geographic map showing the location of Larnaca Lowlands shelf and eastern Mesaoria Basin in southeastern Cyprus. V-F- 4, 7 and 9 are locations of samples analysed by Vita-Finzi (1990) that are discussed in the text. Also shown are the locations of Dhekelia Bay (DB), Ormideia Valley (OV) and Pissouri Basin (P); the black line marks the trace of cross section shown in Figure 2, and the black rectangle shows the approximate boundary of the geologic map of Figure 3.

traceable around the southern two-thirds of the island. In Larnaca, they measured a section at *c.* 8–11 m above SL comprising a basal conglomerate overlain by calcarenite overlain by conglomerate beds; and at Dhekelia Bay (see Fig. 2 for location), they measured a section from *c.* 0 to 3 m above SL of two calcarenite beds separated by a conglomerate bed. U-series age data by Poole *et al.* (1990) and Poole and Robertson (1991) for these beds are discussed in the following section on the Vikla beds.

The eastern Mesaoria Basin lies *c.* 15 km to the north of the Larnaca Lowlands (Fig. 2). There has been little prior geologic work in the eastern Mesaoria, except for Devillers *et al.* (2002), who describe shallow Holocene marine deposits laid down in an inland bay connected to the Mediterranean Sea by a narrow channel. Their reported ages for these deposits are given below.

Stratigraphic column

The Quaternary marine section in the Larnaca Lowlands is divisible into stratigraphic column based on facies and age (Fig. 5). Basal sand and conglomerate beds form the oldest Pleistocene marine unit, herein called the Vikla beds (informal). The Vikla beds are overlain by deposits of two contemporaneous facies: a finer-grained sediment herein called the Kiti Tower sand (informal) and a coarser-grained sediment herein called the Kashanes gravel (informal). Holocene marine sand and gravel deposits occur along the present coast at elevations of +2–3 m and lower. Holocene lagoon and shallow-water marine deposits occur beneath the salt lakes at elevations of SL and lower.

Vikla beds – basal Late Pleistocene section: MIS-5–7

The Vikla beds is our proposed name for basal Late Pleistocene marine sediments that crop out at scattered locations on the Larnaca Lowlands shelf. The name comes from Vikla Point – a prominent ledge on the south side of Larnaca. This unit is an assemblage of time-transgressive sediments that have accumulated on the shelf over the course of tens of thousands of years. These deposits rest with angular unconformity on the Nicosia Formation at

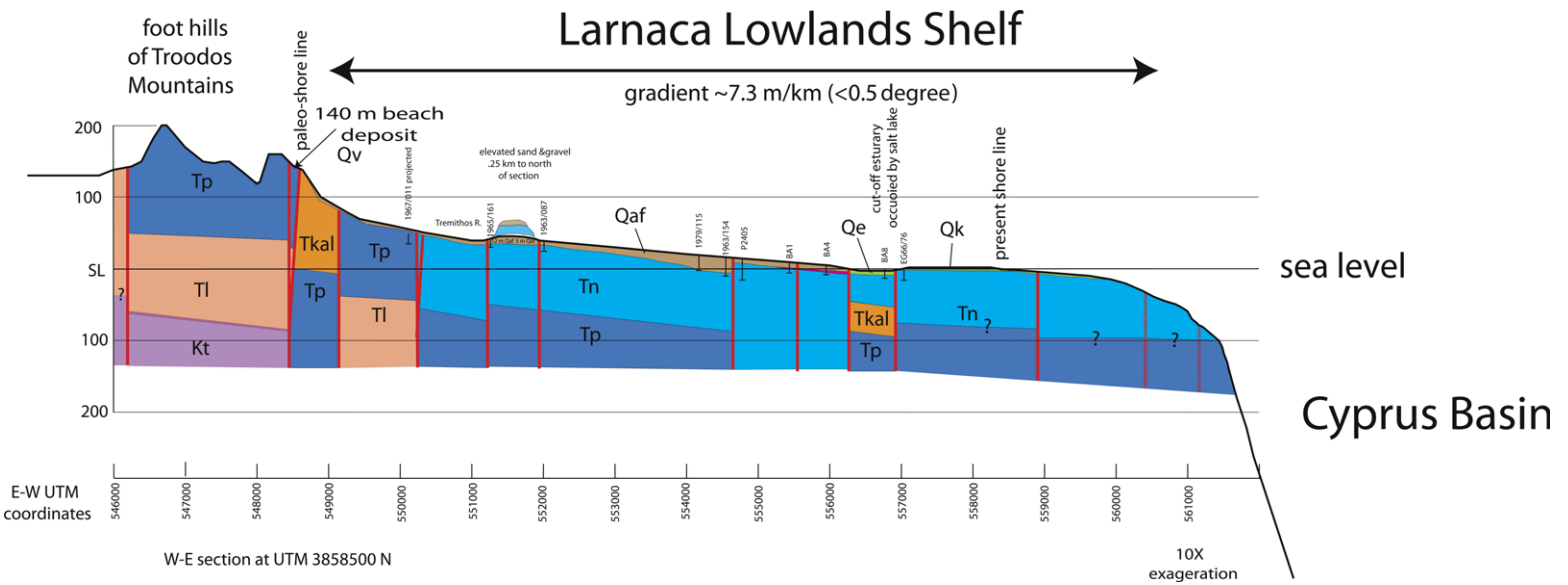

Fig. 3. East to west cross section across the Larnaca Lowlands shelf at the latitude of the Larnaca International Airport; 10× exaggeration. Units shown from oldest to youngest are: Kt, Cretaceous Troodos Ophiolite Complex; Tl, Palaeogene Lefkara Formation; Tp, Miocene Pakhna Formation; Tkal, Late Miocene; Messinian Kalavasos Formation; Tn, Late Miocene to Early Pleistocene Nicosia Formation; Qaf, Late Pleistocene alluvial fan deposits; Qk, Late Pleistocene Kashanes gravel; Qkts, Late Pleistocene Kiti Tower sand; Qm, Holocene marine sand and beach gravel; Qe, Holocene estuarine deposits in cut-off estuary.

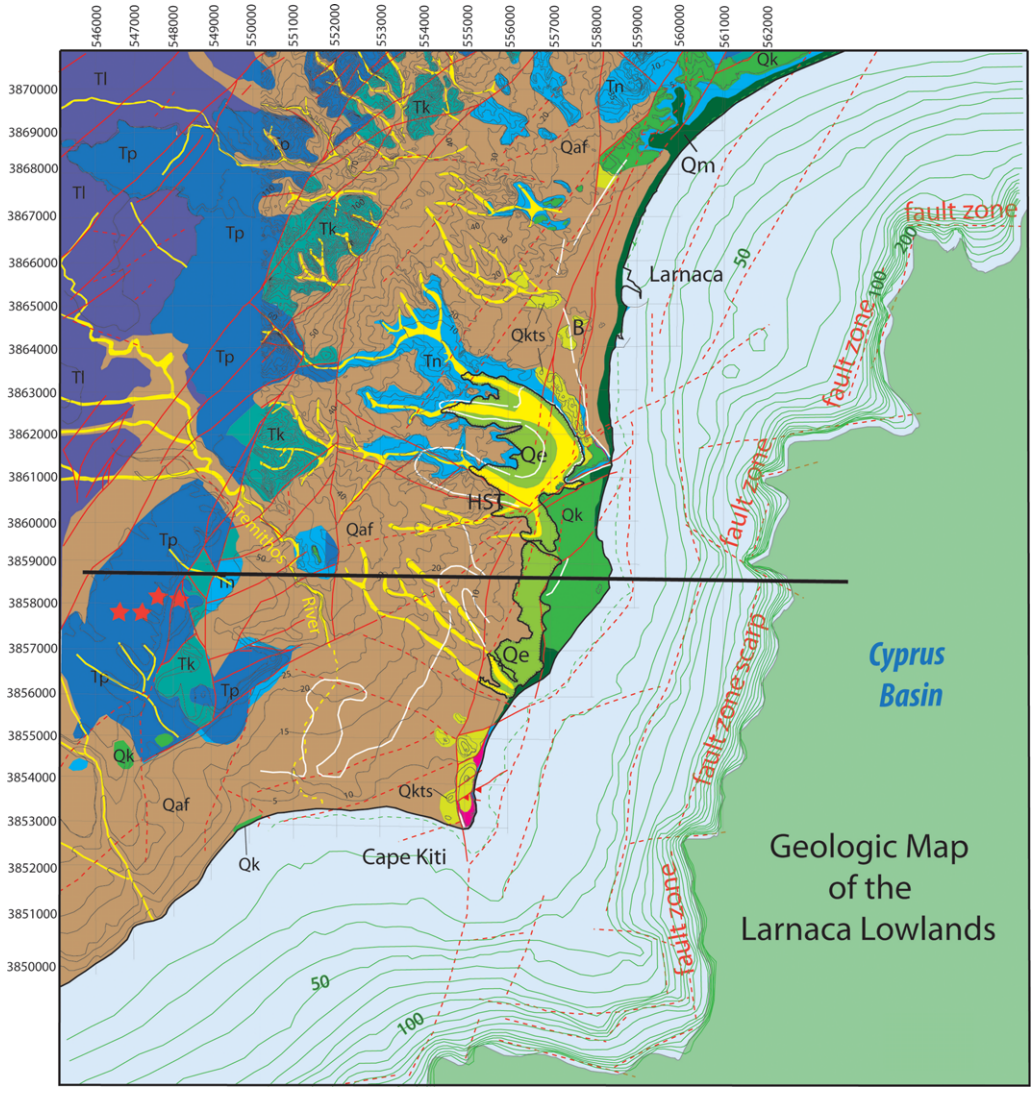

Fig. 4. Geologic map of the central portion of the Larnaca Lowlands. Line of section shown in Figure 3 is marked by the black line. White line is a structural contour at SL for the top of Pliocene substrata. Units are the same as those shown in Figure 3. Red stars are locations of 140–160 m oyster-bearing near-shore deposits. HST, Hala Sultan Tekke; B, Bamboula.

Dhekelia Bay and the Larnaca area and on the Pakhna Formation at Cape Kiti. They comprise intercalated, thin, lithic sand and conglomerate beds. Gifford (1978) showed that marine sand of the Vikla beds at +3 m elevation in Larnaca has a sorting profile identical to that found in the swath zone of modern Mediterranean beaches. Clasts consist of mafic–ultramafic rocks (Troodos Ophiolite), chalk and chert fragments that are typically well rounded to disc-shaped. Beds vary from very fossiliferous at Dhekelia Bay to sparsely fossiliferous at Larnaca and at Cape Kiti. At Dhekelia Bay, Vikla beds are overlain by burrowed sand of the Kiti Tower sand, which is overlain by gravel and sand beds of the Kashanes gravel (both are discussed below). In the Cape Kiti area, strongly calichified, sparsely to non-fossiliferous Vikla beds lie on Miocene Pakhna Formation and are overlain by Kiti Tower sand.

Also assigned to Vikla beds are marine sand and gravel beds that occur at 140–160 m in elevation at several locations surrounding the Larnaca Lowlands. These deposits are interbedded, well-sorted,

Table 1. *^{14}C data*

Laboartory ID	Field sample ID	Material	UTM *x*-axis	UTM *y*-axis	Altitude	$\delta^{13}C$	±	^{14}C age	Calibrated age (2σ)	Mean
Kashanes gravel										
USGS WW7204	2/9/09-1	Bivalve shell	558380	3859050	0	1.89	540	37 670	41 267–42 817	42 042 ± 775
USGS WW7210	2/9/09-12	Bivalve shell	555186	3852800	3	1.31	450	36 090	39 615–41 732	40 674 ± 1059
USGS WW7799	11/15/09-3	Bivalve shell	558245	3859115	1	−0.2	100	22 110	25 581–26 362	25 972 ± 391
USGS WW7800	11/15/09-6	Bivalve shell	558245	3859115	1	1.14	450	34 900	38 575–40 744	39 660 ± 1085
USGS WW7801	11/18/09-8	Bivalve shell	557500	3860950	0	2.57	380	33 030	36 523–38 451	37 487 ± 964
USGS WW7802	11/18/09-9	Gastropod shell	557500	3860950	0	1.91	180	27 370	31 086–31 510	31 298 ± 212
USGS WW7807	11/19/09-1	Gastropod shell	556769	3860507	0	1.64	100	22 390	26 025–26 831	26 428 ± 403
USGS WW7811	11/18/09-5	Fossil algae	557500	3860950	0	1.17	530	36 250	39 621–41 929	40 775 ± 1154
USGS WW7812	11/18/09-7	Bivalve shell	557500	3860950	0	1.49	1200	42 800	43 885–48 460	46 173 ± 2288
USGS WW7841	11/19/09-2	Spondylus bivalve	556775	3860408	0	2.35	520	37 380	41 088–42 614	41 851 ± 763
USGS WW7845	11/20/09-1	Bivalve shell	555088	3852774	5	1.85	360	34 360	37 630–40 035	38 833 ± 1203
USGS WW7846	11/20/09-7	Bivalve shell	555340	3854010	1	o.87	600	38 410	41 665–43 411	42 538 ± 873
USGS WW7848	11/20/09-6	Bivalve shell	555317	3853962	2	2.3	440	35 830	39 311–41 502	40 407 ± 1096
USGS WW8054	2/21/10-6*	*In situ* coral colony	557527	3861164	0	−3.82	270	31 680	35 100–36 449	35 775 ± 675
USGS WW8055	2/21/10-8	Bivalve shell	557478	3861017	5	3.23	450	36 090	39 615–41 732	40 674 ± 1059
USGS WW8056	2/24/10-1	Bivalve shell	555115	3852762	8	0.99	290	32 700	36 275–37 780	37 028 ± 753
USGS WW8058	2/28/10-3	Bivalve shell	561973	3870572	5	−2.76	1100	43 300	44 429–48 679	46 554 ± 2125
USGS WW8059	2/28/10-5	Bivalve shell	566900	3871416	5	0.62	1100	43 200	44 355–48 585	46 470 ± 2115
USGS WW8122	11/15/09-10*	Gastropod shell	558248	3861315	9	1.74	350	30 820	34 480–35 596	35 038 ± 558
USGS WW8123	11/21/09-6	Bivalve shell	556047	3865503	14	2.11	350	37 820	41 602–42 705	42 154 ± 552
USGS WW8195	5/25/10-1	Shell hash	559919	3869209	3	1.06	330	33 420	36 765–38 610	37 688 ± 923
USGS WW8196	5/22/10-1	*In situ* coral	550246	3852933	1	−3.24	210	29 860	33 446–34 648	34 047 ± 601
USGS WW8199	5/27/10-1	Strombus shell	549761	3852781	1	1.66	450	36 030	39 532–41 680	40 606 ± 1074
USGS WW8200	5/29/10-1*	Clam shell half	562802	3871263	7	1.16	490	36 760	40 523–42 189	41 356 ± 833
USGS WW8201	5/29/10-2	Clam shell whole	566901	3871361	3	1.1	380	34 710	38 511–40 476	39 494 ± 983
USGS WW8202	5/29/10-3	*In situ* coral	567155	3871296	1	−2.85	660	39 150	42 117–44 150	43 134 ± 1017
USGS WW8203	5/29/10-4*	Bivalve shell	567155	3871296	1	0.87	860	41 350	43 264–45 863	44 564 ± 1300
USGS WW8206	6/3/10-1	Coral	557727	3861719	10	−2.24	420	35 410	38 952–41 079	40 016 ± 1064
Kiti Tower sand										
USGS WW7844	11/19/09-7	Shell hash	554685	3853528	5	1.05	420	35 380	38 932–41 051	39 992 ± 1060
USGS WW7850	11/21/09-4	*In situ* whole clam	556913	3865102	7	1.66	630	38 900	41 974–43 944	42 959 ± 985

(*Continued*)

Table 1. *Continued*

Laboartory ID	Field sample ID	Material	UTM *x*-axis	UTM *y*-axis	Altitude	$\delta^{13}C$	±	^{14}C age	Calibrated age (2σ)	Mean
USGS WW8124	3/02/10-1	Bivalve shell (F)	580632	3889671	8	1.54	390	37 320	41 215–42 405	41 810 ± 595
USGS WW8125	3/02/10-2	Shell hash (F)	580632	3889671	9	−0.22	390	38 560	42 020–43 211	42 616 ± 596
USGS WW8192	11/21/09-5A*	*In situ* whole clam	556909	3865124	5.5	1.49	1000	42 700	44 071–47 682	45 877 ± 1806
USGS WW8193	11/21/09-5B*	*In situ* whole clam	556909	3865124	5.5	1.17	1600	46 400	46 199–49 900	48 050 ± 1851
USGS WW8204	6/2/10-3	Shell hash (F)	580557	3889279	8	−7.36	440	35 770	39 240–41 444	40 342 ± 1102
Terraces, west Cyprus										
SRR-3241	Vita-Finzi (1990)-4	*Glycymeris violasecens*	35° 03′ N	32° 21′ E	7	1.7	1140	39 330	41 909–45 120	43 515 ± 1606
SRR-3239	Vita-Finzi (1990)-7	*Monodonia turbinate*	35° 11′ N	32° 27′ E	12	−2.1	710	39 330	42 435–44 561	43 498 ± 1063
SRR-3238	Vita-Finzi (1990)-9a	*Glycymeris violasecens*	34° 49′ N	32°23′ E	10	−0.1	400	32 750	36 257–38 395	37 326 ± 1069
SRR-3243	Vita-Finzi (1990)-9b	*Spondylus sp.*	34°50′ N	32°24′ E	5.5	0.9	600	31 110	34 402–36 580	35 491 ± 1089
SRR-3244	Vita-Finzi (1990)-9d	*Glycymeris sp.*	34° 50′ N	32° 24′ E	3.6	0.2	310	30 270	33 599–35 052	34 326 ± 727
Holocene marine Salt Lakes Estuary										
USGS WW7842	11/19/09-3	*In situ* coral colony	556775	3860408	0	−2.25	30	5160	5454–5584	5519 ± 65
Gifford (1978)	K11	Organic, lagoon	*c.* 554796	*c.* 3861120	−5.5	Not reported	125	6345	6950–7484	7217 ± 267
Gifford (1978)	K13	Organic, lagoon	*c.* 555143	*c.* 3861060	−10.8	Not reported	170	6065	6530–7312	6921 ± 391
Gifford (1978)	K16	Organic, lagoon	*c.* 556265	*c.* 3856140	−6.5	Not reported	105	5270	5886–6286	6086 ± 200
GSD Cyprus	BH69/76	Organic, lagoon	*c.* 556469	*c.* 3859090	−7.8	Not reported	115	4130	4349–4884	4617 ± 268
Coastal deposits										
USGS WW7865	11/21/09-2	Organic mass	558151	3865667	0	−16.79	35	2075	1539–1756	1648 ± 109
USGS WW7866	11/21/09-3	Organic mass	558151	3865667	0	−16.74	35	2115	1591–1808	1700 ± 109
USGS WW7843	11/19/09-5	Bivalve shell	555993	3855438	1	1.85	35	3520	3319–3506	3413 ± 94
USGS WW7205	2/9/09-2	Bivalve shell	558380	3859050	0.5	2.5	30	3790	3632–3829	3731 ± 99
USGS WW7206	2/9/09-3	Bivalve CK fault zone	555180	3852800	0.5	−1.15	35	6580	6989–7208	7099 ± 110

USGS WW7209	2/9/09-10	Bivalve CK beach	555185	3852800	3.5	1.4	35	6930	7363–7520	7442 ± 79	
Gifford (1978)	K3	Organic mass	*c.* 558000	*c.* 3864800	−1.3	Not reported	85	2215	1988–2361	2175 ± 187	
Gifford (1978)	K7	Organic mass	*c.* 558041	*c.* 3864180	−2.8	Not reported	100	2540	2350–2,792	2571 ± 221	
Gifford (1978)	K8	Organic mass	*c.* 557620	*c.* 3863600	−2.3	Not reported	120	3121	2994–3615	3305 ± 311	
Morhange *et al.* (2000)	CVI 1	Organic, Posidonia	*c.* 557633	*c.* 3864380	−2.4	−22.63	45	3015	2704–2894	2799 ± 95	
Morhange *et al.* (2000)	CVI 6	Organic, Posidonia	*c.* 557633	*c.* 3864380	−1.9	−20.02	60	2135	1561–1866	1174 ± 153	
Morhange *et al.* (2000)	CVIII 6	Lagoonal clay	*c.* 557755	*c.* 3864420	−1.6	−20.47	40	1620	1076–1269	1173 ± 97	
Morhange *et al.* (2000)	CXI 10	Organic, Posidonia	*c.* 558102	*c.* 3864560	−7.7	−16.55	60	3865	3644–3992	3818 ± 174	
Morhange *et al.* (2000)	CXI 2	Organic, Posidonia	*c.* 558102	*c.* 3864560	−6	est. *c.* −15	60	2655	2151–2540	2346 ± 195	
Morhange *et al.* (2000)	CXII 15	Organic, Posidonia	*c.* 557918	*c.* 3864820	−6.3	−14.31	50	4320	4292–4599	4446 ± 1535	
Yon (1994)		Marine shell			*c.* 3	Not reported	50	4830	4963–5277	5120 ± 157	
Alluvial fan deposits											*3 ka correction*
USGS WW7809	11/18/09-3	Terrestrial snail shell	554963	3864211	20	−6.89	530	40 600	43 486–45 276	44 381 ± 895	*c.* 41 000 ± 1000
USGS WW8057	2/25/10-1	Terrestrial snail shell	552435	3867810	67	−8.33	30	7760	8454–8594	8524 ± 70	*c.* 5500 ± 100
USGS WW8194	6/1/10-3	Terrestrial snail shell	580557	3889279	12	−9.3	35	4225	4696–4760 (41%)	4728 ± 32	*c.* 1700 ± 50
USGS WW7810	11/18/09-4	Bedded caliche	554963	3864211	21	−6.03	30	10 800	12 578–12 810	12 694 ± 116	
Gifford (1978)	HST:Area 22	Caliche soil	*c.* 555296	*c.* 3860680	>5		450	15 860	18 426–20 033	19 230 ± 804	

All samples with control numbers beginning in WW were processed at the ^{14}C laboratory of the US Geological Survey in Reston, Virginia and ^{14}C ages were determined at the Center for Accelerator Mass Spectrometry, Lawrence Livermore National Laboratory, Livermore, California. All other samples and corresponding ages in this table originated in other publications and are listed here for comparison. Radiocarbon ages reported in years before Present (year bp) were calculated using the Libby half-life of 5568 years. Values reported for $\delta^{13}C$ are given in parts per million (‰) relative to the Pee Dee Belemnite standard. Those reported with decimal places were measured for the material itself; all others are estimates. The $\delta^{13}C$ values marked 'not reported' indicate that this information was not included in the original publication. Calibrated ages are given as two-sigma (2σ) ranges and the mean values of those ranges in years BP using the IntCal09 and Marine09 calibration curves (Reimer *et al.* 2009) for terrestrial and marine samples, respectively, in conjunction with the Calib 6.0 radiocarbon calibration program (Stuiver & Reimer 1993). Bracketed values indicate that the calibrated range impinges upon the end of the calibration data set. For the three terrestrial snail samples, 3000 years was subtracted from the reservoir age before calibration to adjust for the maximum error found in land snails (see Harrison *et al.* (2008) for background on dating of the same snail species from Cyprus & Goodfriend (1987) for calibration throughout Middle East). Ages of the six samples whose initial radiocarbon values approach the limitations of the technique at *c.* 45 ka could represent minimum values. Samples marked with an asterisk showed only trace amounts of aragonite recrystallization to calcite (<1%) when analysed by XRD and are 99–100% aragonite; unmarked samples analysed showed 95–98% aragonite and 2–5% calcite.

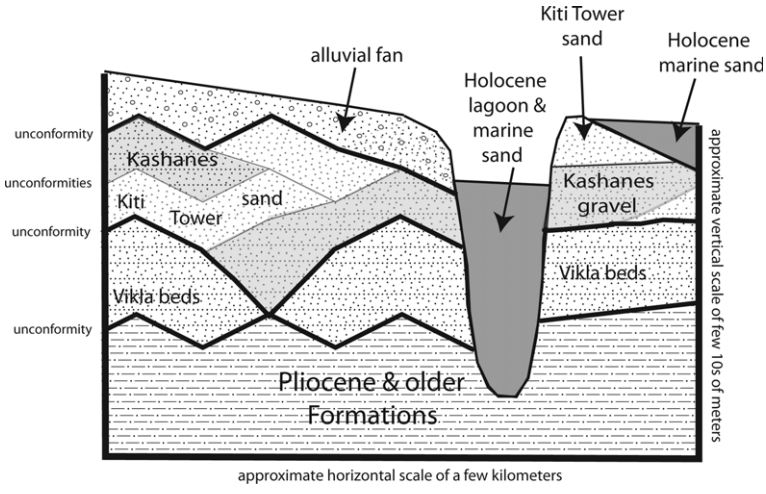

Fig. 5. Stratigraphic column for Late Pleistocene and Holocene units found on the Larnaca Lowlands shelf, SE Cyprus.

strongly indurated sand and pebbly gravel beds that are similar to Holocene coastal sediments along the present shoreline; thickness is as much as 10 m. Clasts are from all older units; flattened disc-shape clasts are common. Oyster shells occur sporadically.

Poole *et al.* (1990) and Poole & Robertson (1991) report U-series ages on *Cladocora caespitosa* coral from the Vikla beds at Vikla Point of 183 ± 2, 209 ± 7, 197 ± 16 and 183 ± 12 ka and at Dhekelia Bay of 113 ± 3, 122 ± 3, 123 ± 3, 132 ± 7, 135 ± 4 and 138 ± 4 ka. Their spread in ages is interpreted to be the result of reworking and accumulation of coral death assemblages during MIS-5–7, prior to lithification. We acquired three optically stimulated luminescence (OSL) ages from sand beds in the Vikla beds of *c.* 85 000, 88 200 ± 4760 and 175 000 ± 7600 (Table 2) from elevations of 9, 30 and 48 m above SL, respectively. An oyster shell from the 140–160 m deposits analysed by ^{14}C yielded a carbon-dead, >54,000 calibrated years bp (cal-year-bp; Table 1).

Kiti Tower sand and Kashanes gravel: MIS-3 and 4 marine deposits

Overlying the Vikla beds are deposits of two contemporaneous marine facies. These are a sand-dominated facies that we call the Kiti Tower sand and a coarser facies of intercalated gravel and minor sand that we call the Kashanes gravel. These sediments crop out in a nearly continuous 2–3 km-wide belt along the coast of the Larnaca Lowlands (Fig. 4).

Kiti Tower sand. Kiti Tower sand is our name for exposures around the Medieval Kiti Tower, which is located *c.* 2 km north of Cape Kiti. Typically, this formation comprises weakly to moderately indurated, coarse- to medium-grained lithic sand. Characteristics of this unit vary locally from massive to thin bedding and from cross-bedded foreset beds to planar, strongly burrowed beds. Lithic grains comprise chalk, chert and mafic–ultramafic material. Quartz grains are very sparse and may be of aeolian origin blown in from Africa. Reworked foraminifera from older Cenozoic units are common to abundant. Indigenous macrofossils are relatively sparse, but locally whole clams in death position occur in massive sand beds, and thin beds of broken shell hash are common in higher-energy cross-bedded sediments.

Kiti Tower sand crops out at elevations of SL to as much as +30 m north of Cape Kiti and in Larnaca, but is absent between these areas (Fig. 3). Excavations within Larnaca reveal unconformities within the Kiti Tower sand that represent regressive–transgressive cycles (Fig. 6). Kiti Tower sand also crops out in beach-front cliffs at Dhekelia Bay, where it lies beneath gravels of the Kashanes gravel (described below). Kiti Tower sand also occurs extensively in the eastern Mesaoria Basin (Fig. 2) to the NE of the Larnaca Lowlands shelf.

Our mean age determinations for the Kiti Tower sand range from *c.* 65 ka to *c.* 25 ka bp (see Tables 1 & 2 and Fig. 7). This range is from combined ^{14}C (seven samples) and OSL (10 samples) data, which show overall agreement for these units. OSL ages do show a slightly older range for the Kiti Tower sand, beyond the 50–54 ka upper age limit of the radiocarbon technique (Trumbore 2000). Our ^{14}C ages for the Kiti Tower sand are from various sea shells that include *in situ* whole

Table 2. *Optically stimulated luminescence infrared stimulated luminescence data*

Field and laboratory sample no.	Material	UTM *x*-axis	UTM *y*-axis	Altitude	K (%)	Th (ppm)	U (ppm)	Water (%)	Cosmic dose rate (Gy/ka)	Total dose rate (Ga/ka)	D_e (Gy)	*n*	±	Age (ka)
Vikla beds														
11/15/09-14	Fine-grained sand and gravel	557669	3862548	9	0.43 ± 0.02	1.29 ± 0.23	0.91 ± 0.11	6 (33)	0.20 ± 0.01	0.82 ± 0.07	*c.* 70	2 (9)		*c.* 85 000
3/1/10-3	Fine-grained sand and gravel	567706	3872288	30	0.40 ± 0.02	0.79 ± 0.05	0.63 ± 0.04	11 (31)	0.22 ± 0.02	0.75 ± 0.03	66.2 ± 2.72	17(26)	4760	88 200
3/1/10-4	Fine-grained sand and gravel	567747	3872606	48	0.28 ± 0.01	0.33 ± 0.06	0.23 ± 0.03	12 (34)	0.22 ± 0.02	0.52 ± 0.03	91.1 ± 4.01	14(19)	11 700	175 000
Kashanes gravel														
11/21/09-9	Medium-grained marine sand	556047	3865503	15	0.26 ± 0.02	0.54 ± 0.13	0.68 ± 0.09	1 (30)	0.22 ± 0.02	0.62 ± 0.06	28.4 ± 1.14	18 (25)	5050	45 900
Kiti Tower sand														
4/9/07-2	Medium-grained marine sand	555186	3852800	3	0.39 ± 0.01	0.55 ± 0.09	0.38 ± 0.04	24 (78)	0.19 ± 0.02	0.56 ± 0.03	<15.4 ± 1.69	3 (5)	3450	<27 700
2/9/09-11	Medium-grained marine sand	555184	3852800	3	0.44 ± 0.03	0.93 ± 0.16	0.46 ± 0.09	24 (42)	0.19 ± 0.02	0.69 ± 0.03	23.2 ± 0.31	13 (15)	1700	33 600
2/9/09-4	Medium-grained marine sand	555181	3852800	1	0.24 ± 0.02	0.94 ± 0.16	0.63 ± 0.13	12 (26)	0.14 ± 0.01	0.46 ± 0.02	16.4 ± 0.20	19 (25)	1700	35 700
11/20/09-2	Burrowed sand	555099	3852787	5.5	0.26 ± 0.02	0.87 ± 0.11	0.37 ± 0.04	1 (24)	0.18 ± 0.01	0.55 0.04	23.1 ± 0.94	16 (25)	5940	42 400
11/19/09-8	Burrowed sand	554677	3853039	4	0.22 ± 0.1	0.36 ± 0.07	0.34 ± 0.05	5 (11)	0.22 ± 0.02	0.51 ± 0.04	28.1 ± 2.14	9 (14)	6090	54 900
11/15/09-12	Bioclastic, burrowed sand	557806	3861757	8	0.45 ± 0.02	0.86 ± 0.10	0.70 ± 0.05	4 (38)	0.22 ± 0.02	0.78 ± 0.04	51.2 ± 7.32	7 (15)	9850	65 600
11/15/09-1	Bioclastic, burrowed sand	555244	3854628	14	0.40 ± 0.20	0.82 ± 0.13	0.62 ± 0.06	4(41)	0.22 ± 0.02	0.71 ± 0.05	30.7 ± 4.21	8(15)	6530	43 400
2/23/10-1	Bioclastic, burrowed sand	556933	3865101	15	0.64 ± 0.05	0.71 ± 0.05	0.31 ± 0.02	11 (40)	0.22 ± 0.02	0.90 ± 0.04	40.7 ± 9.36	3(3)	10 600	42 200
3/2/10-3	Bioclastic, burrowed sand	580551	3889560	12	1.00 ± 0.02	0.94 ± 0.08	1.08 ± 0.06	4 (31)	0.22 ± 0.02	1.34 ± 0.04	32.8 ± 3.94	13(22)	3050	24 500
Holocene marine														
11/19/09-6	Coarse-grained marine sand	557059	3856443	1.5	0.31 ± 0.01	0.41 ± 0.09	0.33 ± 0.06	4 (22)	0.18 ± 0.01	0.53 ± 0.04	1.79 ± 0.20	12 (24)	470	3410
11/19/09-4	Burrowed sand	555993	3855438	1	0.52 ± 0.02	1.02 ± 0.20	0.39 ± 0.07	6 (19)	0.22 ± 0.02	0.80 ± 0.07	1.90 ± 0.19	11 (21)	320	2380
Alluvial-fan deposits														
2/9/09-9	Fine-grained alluvium	555180	3852800	3	0.70 ± 0.04	2.25 ± 0.13	0.79 ± 0.07	13 (42)	0.22 ± 0.02	1.08 ± 0.04	18.1 ± 0.49	15 (25)	850	16 700

(*Continued*)

Table 2. *Continued*

Field and laboratory sample no.	Material	UTM *x*-axis	UTM *y*-axis	Altitude	K (%)	Th (ppm)	U (ppm)	Water (%)	Cosmic dose rate (Gy/ka)	Total dose rate (Ga/ka)	D_e (Gy)	*n*	±	Age (ka)
2/10/05-1	Fine-grained alluvium	555180	3852800	3	0.54 ± 0.03	2.05 ± 0.11	0.63 ± 0.04	10 (34)	0.19 ± 0.02	0.88 ± 0.03	13.2 ± 0.43	20 (35)	1350	13 800
2/10/05-2	fine-grained alluvium	555180	3852800	2.5	0.52 ± 0.05	1.89 ± 0.15	0.59 ± 0.05	11 (35)	0.18 ± 0.02	0.90 ± 0.05	18.6 ± 0.55	13 (30)	2430	20 600
4/9/07-1	Fine-grained alluvium	555178	3852800	2	0.31 ± 0.01	1.27 ± 0.11	0.45 ± 0.06	12 (27)	0.16 ± 0.01	0.60 ± 0.03	>18.2 ± 9.05	3 (4)	13 700	>30 300
2/9/09-6	Fine-grained alluvium	555180	3852800	2	0.20 ± 0.02	0.86 ± 0.15	0.41 ± 0.09	17 (40)	0.19 ± 0.02	0.48 ± 0.02	12.4 ± 0.29	16 (25)	1200	25 900
11/18/09-2	Sand lens in gravel	555512	3861766	6	1.19 ± 0.11	0.89 ± 0.13	0.52 ± 0.08	3 (38)	0.22 ± 0.02	1.35 ± 0.08	1.20 ± 0.30	15 (24)	230	900
11/18/09-6	Fine-grained alluvium	555093	3859348	17	1.57 ± 0.11	1.31 ± 0.24	0.41 ± 0.11	3 (24)	0.22 ± 0.02	1.69 ± 0.11	24.6 ± 1.59	13 (18)	1330	14 600
4/9/07-5	Coarse-grained pebble, sand	555182	3852800	2.5	0.44 ± 0.02	1.65 ± 0.19	0.58 ± 0.10	5 (50)	0.19 ± 0.02	0.74 ± 0.05	2.64 ± 0.19	10 (14)	310	3520
4/9/07-3	Coarse-grained pebble, sand	555182	3852800	2	0.20 ± 0.01	0.58 ± 0.08	0.34 ± 0.04	2 (16)	0.19 ± 0.02	0.48 ± 0.03	7.54 ± 0.17	10 (15)	1180	15 600
2/9/09-7	Coarse-grained pebble, sand	555181	3852800	2	0.20 ± 0.01	0.94 ± 0.11	0.37 ± 0.07	3 (23)	0.19 ± 0.02	0.50 ± 0.04	8.50 ± 0.31	10 (20)	1.44	17 000
12/13/06-1	Fine- to medium-grained sand	555179	3852800	2	0.23 ± 0.02	0.73 ± 0.06	0.36 ± 0.03	8 (35)	0.19 ± 0.02	0.49 ± 0.04	6.14 ± 0.32	15 (30)	1250	12 500
12/13/06-2	Fine- to medium-grained sand	555179	3852800	2	0.44 ± 0.03	0.65 ± 0.05	0.60 ± 0.05	15 (41)	0.14 ± 0.01	0.63 ± 0.05	6.93 ± 0.32	15 (20)	1090	12 100

All samples were processed and analysed at the USGS laboratory in Denver, CO except for 6/2/10–2, which was analysed by G. Brook at University of Georgia facilities. Field moisture, with numbers in parentheses indicating the complete sample saturation percentage. Ages calculated using *c.* 90% of saturation values if below the water table. Analyses obtained using laboratory gamma spectrometry (high-resolution Ge detector). Cosmic doses and attenuation with depth were calculated using the methods of Prescott & Hutton (1994). Number of replicated equivalent dose (D_e) estimates used to calculate the mean. Numbers in parentheses indicate total number of measurements made, including runs with unusable data. Dose rate and age for finer-grained 180–190 μm quartz sand. Linear + exponential fit used on equivalent dose, errors to 1σ, single aliquot regeneration. IRSL from fine grains of 4–11 μm, as a check on quartz. Exponential fit used for equivalent dose. Errors to 1σ. Fade tests indicate 3–7% correction.

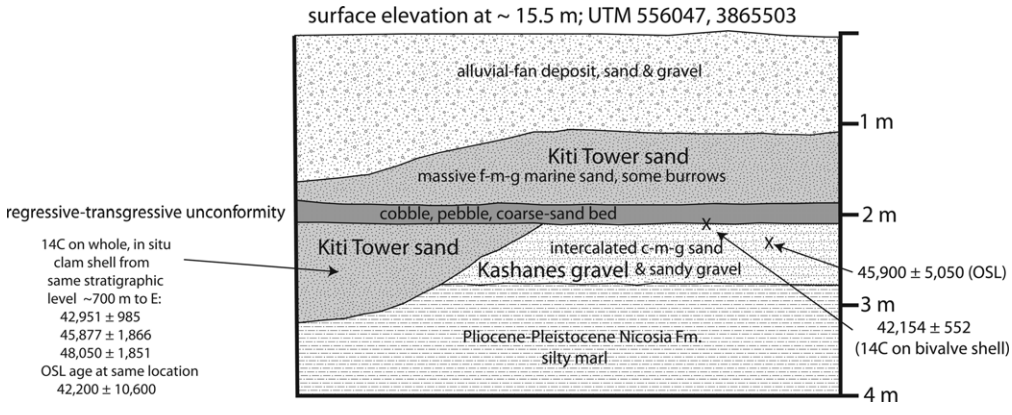

Fig. 6. Drawing of section exposed in a 2009 excavation within the city of Larnaca at UTM coordinates 556047E, 3865503N. Ages are in year bp (see Tables 1 & 2 for geochronology data).

clams and other bivalves. X-ray diffraction (XRD) analyses show only minor amounts of aragonite recrystallization to calcite (>95% aragonite) for five of the ^{14}C-dated samples; two samples of whole, *in situ* clams contained only trace amounts of calcite (>99% aragonite). Excavation for a new school in 2009 exposed a >5 m section of Kiti Tower sand that contained whole *in situ* clams. Our ^{14}C ages for a clam collected at *c.* 7.0 m above SL in this section is 42 974 ± 986 cal-year-bp, and for two clams collected at *c.* 5.5 m above SL are 45 877 ± 1806 and 48 050 ± 1851 cal-year-bp. We obtained an OSL age of 42.2 ± 10.6 ka for a sample collected at *c.* 6.5 m above SL at the same site, demonstrating a very good agreement between the two geochronology techniques and giving us great confidence in the accuracy of our age data. Three of our ages for Kiti Tower sand come from the eastern Mesaoria Basin and they are indistinguishable from ages of this unit from the Larnaca Lowlands, indicating contemporaneous and similar depositional environments at these localities. In good agreement with our ages, an OSL age of 37.4 ± 7.4 ka was obtained for this unit by T. Kinnaird (oral commun., 2011) as part of his PhD.

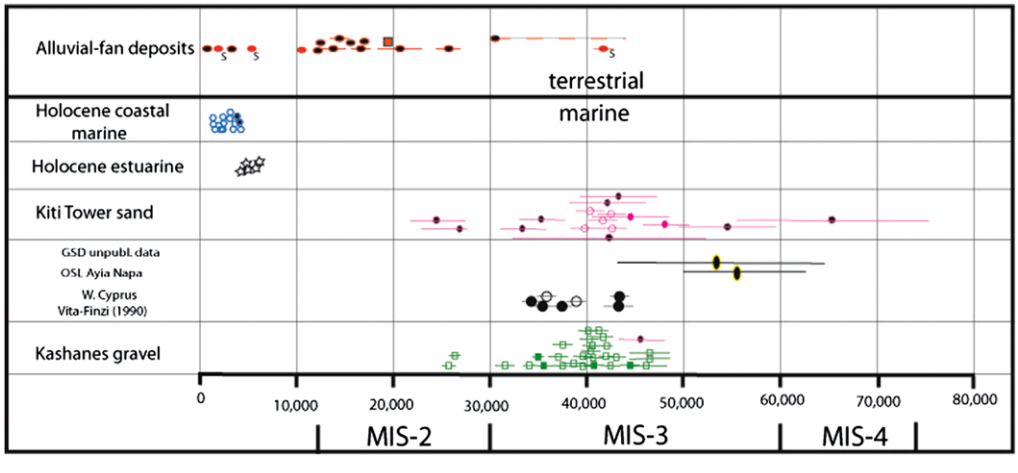

Fig. 7. Plot of ^{14}C and OSL-IRSL geochronology data for the Larnaca Lowlands shelf (from this report, and Gifford (1978), Morhange *et al.* (2000)), eastern Mesaoria Basin (from this report), and sites along the western coast of Cyprus reported by Vita-Finzi (1990). Black-filled symbols are OSL/IRSL ages. All others are calibrated ^{14}C ages; color-filled ^{14}C symbols for Kashanes gravel and Kiti Tower sand are samples that analysed 99–100% aragonite and unfilled ^{14}C symbols analysed 95–98% aragonite. See Tables 1 and 2 for analytical data. 'S' by alluvial-fan deposit age indicates that sample was a terrestrial snail (see text for discussion). Orange-filled box in alluvial-fan ages is a ^{14}C age from Gifford (1998).

Kashanes gravel. Kashanes gravel is our name for marine gravel and sand facies that are intercalated with the Kiti Tower sand. The name is taken from Kashanes Point on the coast near the east side of the Larnaca International Airport, where indurated, fossiliferous gravel and sand beds crop out from SL to *c.* 2 m above SL and are unconformably overlain by unconsolidated Holocene sand. The outcrop pattern of this unit is very similar to that of the Kiti Tower sand from Dhekelia Bay to Cape Kiti. Kashanes gravel also crops out on the southern coast *c.* 5 km west of Cape Kiti.

Clasts in Kashanes gravel comprise cobbles, granules and sand of chert, chalk and mafic–ultramafic composition. Cobbles are typically rounded to well rounded and matrix supported. Some clasts are disc shaped. Beds vary from thin (few centimetres) to massive (>1–2 m) and are typically poorly to moderately sorted. The unit varies from very fossiliferous to sparsely fossiliferous. Gaudry (1862) identified 88 species of mollusks, four species of *Serpula*, three varieties of echinoderms, and the coral *Cladocora caespitosa* from beds of Kashanes gravel in the Larnaca area.

We produced ^{14}C ages on 27 marine shells of varied species (not all identified to genus) and spatial distribution from the Kashanes gravel (Table 1). XRD analyses show minor amounts (<5%) of aragonite recrystallization to calcite for 23 of these samples; three samples show trace amounts (<1) of recrystallization, and a sample of coral in growth position shows no recrystallization. Mean values of individual shells range from *c.* 26–46 ka (Fig. 7). There is no distinguishable age difference between samples with minor recrystallization and those with trace amounts or no recrystallization; this is similar to the results of Vita-Finzi (1990). We obtained one OSL age of 45.9 $\pm$ 5.1 ka from a thin sand bed within the Kashanes gravel; this age agrees well with a ^{14}C age of 42 154 $\pm$ 552 cal-year-bp for a shell collected directly over the OSL-dated sample (Fig. 6), again demonstrating the close correlations in ages acquired by these two techniques. The majority of the Kashanes population clusters around 40 $\pm$ 6 ka; the youngest two ages for this unit are *c.* 26–27 ka, which are similar to the youngest ages obtained for the Kiti Tower sand. The similarity in ages between the Kashanes and Kiti Tower units agrees well with observed field relations between these two interbedded facies (Fig. 6).

Other MIS-3 and 4 marine deposits on Cyprus

Our ^{14}C ages on marine shells from Kashanes and Kiti Tower units in the Larnaca Lowlands and eastern Mesaoria Basin overlap ^{14}C ages on marine shells reported by Vita-Finzi (1990) from near-shore marine deposits in western Cyprus (see Fig. 2 for locations of his samples; his analyses are included in Table 1 and are plotted on Fig. 7). Vita-Finzi's (1990) samples came from elevations of *c.* 4–30 m above SL, similar to ours.

Additional data indicating that MIS-3- and 4 marine deposits exist at or above present SL on Cyprus are provided by OSL age constraints on a 6 m-thick bed of calcarenite at Ayia Napa (see Fig. 2), where two samples yielded age ranges of 46.8 $\pm$ 2.6 to 60.9 $\pm$ 4.4 and 53.0 $\pm$ 2.7 to 57.9 $\pm$ 5.2 ka (Geological Survey Department, GSD, Cyprus, 2010). Undated, poorly consolidated marine sand and gravel deposit that crops out in the Ormideia Valley (see Fig. 2) between Ayia Napa and Larnaca appears to be identical to our Kiti Tower and Kashanes units. Also, the undated Pissouri sandstone unit (see Fig. 2) of Stow *et al.* (1995) is considered as possibly correlative with our Kiti Tower sand. The Pissouri sandstone unit is strongly bioturbated and intercalated with widespread gravels and well-developed palaeosols, and locally the unit displays Gilbert-type forest beds (Stow *et al.* 1995). All of these characteristics are similar to the Kiti Tower sand and both units occupy the same stratigraphic interval at the top of the marine section, directly below alluvial-fan deposits. The Pissouri sandstone unit is relatively thick at *c.* 80 m (Stow *et al.* 1995) and occurs at higher elevations than the Kiti Tower sand. We suggest the possibility that the Pissouri Sandstone and our Kiti Tower sand could be equivalent units.

MIS-2 unconformity

The unconformity that bounds the top of the Kiti Tower–Kashanes sequence marks a significant erosional regressive cycle that affected the landscape of the Larnaca Lowlands shelf and eastern Mesaoria Basin. During the period marked by this unconformity, Kiti Tower–Kashanes sediments were raised above SL and there is no indication that they were ever again below SL; we offer this as an explanation as to why shells with minor (<5%) recrystallization yield similar ages to shells with only trace (<1%) to no recrystallization – after deposition, they were never again in a saturated environment. Fluvial valleys were incised through the Late Pleistocene section and into the underlying substratum during the regressive cycle. Subsurface drill data on file at the GSD in Nicosia indicate that the floor of the palaeo-valley beneath the Larnaca Salt Lakes is cut as much as 12 m below present SL; drill data by Gifford (1978) show a depth of incision of *c.* 16 m for this palaeo-valley. Drill data (Devillers

et al. 2002) indicate a palaeo-valley floor of *c.* 20 m below SL in the eastern Mesaoria Basin. Structural contours drawn on the top of substrata in the Larnaca Lowlands shelf (see Fig. 3) reveal two other palaeo-valleys that have been subsequently filled and buried by alluvial fan deposits.

Holocene estuarine deposits beneath the Larnaca Salt Lakes and in the eastern Mesaoria Basin

Holocene estuarine deposits are known to exist beneath the Larnaca Salt Lakes from drill data and ^{14}C dates reported by Gifford (1978), and an unpublished engineering report on the Larnaca International Airport on file at GSD in Nicosia (Gajarda & Makris 1998). These reports describe a marine section that extends from SL to *c.* 16 m below SL and rests upon silt and marl beds of the Nicosia Formation. These marine deposits consist of olive-grey to dark-grey sandy to silty mud deposits that contain varying amounts of shells and organic–marine–plant material. Late Holocene colluvium deposits containing Late Bronze Age and Roman Era sherds and alluvial fill of mud and well-rounded, polished sand and gravel overlie the estuarine deposits (Gifford 1978).

Our mapping of the Larnaca Lowlands discovered *in situ* coral *Cladocora caespitosa* at *c.* 0.5 m above SL on the eastern side of the Main Larnaca Salt Lake. The coral grew attached to gravel of the Kashanes gravel and yielded a ^{14}C age of 5511 $\pm$ 65 cal-year-bp. This age agrees well with ^{14}C ages obtained by Gifford (1978) and GSD, Cyprus on organic material at elevations of *c.* 5.5 to 10.8 m below SL in the estuarine fill of 7217 $\pm$ 267, 6921 $\pm$ 391, 6086 $\pm$ 200, and 4617 $\pm$ 268 cal-year-bp (Table 1 and Fig. 7) . It also agrees well with archaeology data that indicates the Late Bronze age site of Hala Sultan Tekke on the Main Larnaca Salt Lake was built on a marine shore at approximately today's SL (Åström *et al.* 1983). The port of Hala Sultan Tekke was abandoned at *c.* 2500 year bp when the mouth of the estuary was cut off from the sea owing to uplift (Gifford 1978). This uplift ended marine deposition in the estuary; historical data indicate that the Main Larnaca Salt Lake was producing salt at *c.* 2250 year bp and no longer connected to the Mediterranean Sea.

Devillers *et al.* (2002) report *c.* 20 m of fossiliferous Holocene silt and sand, and marine organic material recovered from a drill hole in the eastern Mesaoria Basin (Fig. 2). They interpreted these sediments as having been deposited in a vast estuarine bay and report ^{14}C ages (cal-year-bp) on sea shells of 3805 $\pm$ 165 at *c.* 2.2 m below SL, 4180 $\pm$ 190 at *c.* 6.8 m below SL, 7185 $\pm$ 145 at *c.* 7.7 m below SL, 7400 $\pm$ 150 at *c.* 19.1 m below SL and 8750 $\pm$ 250 at *c.* 19.8 m below SL. Devillers *et al.* (2002) postulate that the ancient seaport of Enkomi was located on the shores of this palaeo-estuary. Today, stone blocks that are thought to be ship moorings at Enkomi are partially excavated at *c.* 4 m above SL, but until further archaeological work is completed, the suggested past SL is considered tentative.

Holocene marine deposits along the Larnaca coast

Unconsolidated Holocene marine sediment occurs along the present shore of the Larnaca Lowlands (Fig. 4). These deposits vary from well to moderately well sorted littoral sand and gravel to silty sand to very poorly sorted, gravelly, muddy sand. In addition to marine fauna, Hellenistic and Roman Era sherds occur within some of these deposits (Gifford 1978; Morhange *et al.* 2000). Drill core obtained for the archaeology studies of Gifford (1978) and Morhange *et al.* (2000) and building excavations in the city of Larnaca encountered beds of organic-rich sediments, consisting mostly of *Posidonia oceanic* fibres, interbedded with the clastic sediments.

Several ^{14}C ages have been obtained previously on the organic layers at Larnaca by Gifford (1978) and Morhange *et al.* (2000); these range from *c.* 1173 to *c.* 4446 cal-year-bp (Table 1 and Fig. 7). Two ^{14}C dates obtained on organic material for this report are 1726 $\pm$ 99 and 1780 $\pm$ 86 cal-year-bp (Table 1, Fig. 7). Our samples came from about present SL and are overlain by *c.* 1 m of marine sand and subsequently by *c.* 1 m of anthropogenic fill. We also obtained a ^{14}C age of 3731 $\pm$ 99 cal-year-bp on bivalve shells collected from Holocene marine sand at 0.5 m above SL that overlies the Kashanes gravel at its type locality and an OSL age of 3440 $\pm$ 620 bp from sandy marine clay at *c.* 1 m near Cape Kiti.

Also, we sampled Holocene marine deposits exposed from SL to *c.* 2 m above SL at the former confluence of the salt lakes estuary and the Mediterranean Sea, from which we obtained a ^{14}C age of 3426 $\pm$ 87 cal-year-bp on a bivalve shell, OSL ages of 3410 $\pm$ 470 and 2380 $\pm$ 320 year bp, and an Infrared Stimulated Luminescence (IRSL) age of 2940 $\pm$ 190 year bp (Tables 1 & 2). These latter ages are consistent with an ^{14}C age of 6023 $\pm$ 264 cal-year-bp determined by Gifford (1978) from drill-core material recovered from 6.5 m below SL at the same locality (sample K16 in Table 1) in that they show a younging-upward sequence of marine deposits.

Late Pleistocene and Holocene alluvial fan deposits

Alluvial fan deposits cover much of the Larnaca Lowlands (Fig. 4). These deposits range from proximal interbedded gravel and coarse-grained-sand facies to distal fine-to-medium-sand and silt facies. They occur at elevations of as much as 120 m above SL to SL along the coast. Thicknesses vary from a few metres to as much as 30–40 m but are mostly less than 20 m. In the northern half of the Larnaca Lowlands, relatively extensive areas are barren of fan deposits and older substrata are at the surface. The alluvial fan deposits grade into thin terrace deposits in strath valleys incised into the western bedrock hills, which are the primary source for the detrital material. Palaeo-flow directions from imbricated clasts are consistently towards the SE and south, similar to present-day stream flow. Included in the alluvial fan deposits shown on the geologic map (Fig. 4) are proximal colluvial-wedge deposits that have been shed off from the adjacent fault-uplifted hills to the west of the lowlands.

Fourteen age determinations for the alluvial fan deposits range from *c.* 42 to <1 ka (Tables 1 & 2, Fig. 7). However, all but two of these ages are ≤25 ka. All but one of the ages were derived from ^{14}C and OSL techniques for this report; the additional age comes from archaeological data of Gifford (1978), who found sherds from *c.* 2 600 year bp incorporated in alluvial fan sediment near the coast at Larnaca. Gifford (1978) also recognized a 20 cm-thick, red-brown palaeosol in the alluvial fan sequence near Hala Sultan Tekke (HST on Fig. 4), for which he obtained a ^{14}C date of 19 230 ± 804 cal-year-bp. Our OSL ages on samples from a *c.* 2 m-thick section of alluvial-fan deposits at Cape Kiti show a downward sequence of 13.8 ± 1.35, 16.7 ± 0.85, 20.6 ± 2.43 and 30.3 ± 13.7 ka. A palaeosol that is similar in thickness and colour to the one dated by Gifford (1978) occurs in the interval between the last two ages in the Cape Kiti sequence. The palaeosols at both Larnaca and Cape Kiti are at <5 m elevation and near the coast. About 3 km inland and at *c.* 17–18 m above SL, an OSL age of 14.6 ± 1.3 ka and an IRSL age of 19.2 ± 1.6 ka were obtained from a sample of sandy mud in alluvial fan deposits directly above a palaeosol that is similar in thickness and colour to the other palaeosols. Occurrences of similar, but undated, palaeosols exist to as much as 120 m above SL in the uplands to the west of the Larnaca Lowlands. An area of youthful, non-dissected fan morphology occurs in the southern third of the Larnaca Lowlands below where the Tremithos River exits the western bedrock hills (Fig. 4).

Discussion: Neogene uplift and mechanisms of crustal uplift

The fact that Cyprus is the only island in the Eastern Mediterranean Sea attests to unique crustal processes there that are different from those of surrounding areas. This uniqueness is further illustrated by gravity studies (Harrison 1955; Gass & Masson-Smith 1963; Ergün *et al.* 2005) that show a pronounced positive anomaly characterizing Cyprus: an anomaly great enough to isostatically require *c.* 1 cm/year of subsidence to maintain equilibrium (Harrison 1955). The source of the anomaly is the massif of the Troodos Ophiolite. Evidence in the sedimentary cover overlying the Troodos indicates that at least portions of the island have been elevated relative to elsewhere in the Eastern Mediterranean as far back at the Early Miocene (Robertson 1977; Eaton 1987). Sedimentary evidence also indicates that, since the Middle Pliocene, much of the island has been above SL and has been episodically rising (McCallum 1989; McCallum & Robertson 1990; Harrison *et al.* 2008). Understanding the nature and causes of this uplift is fundamental in understanding neotectonism along the southern boundary of the Anatolian microplate and the crustal evolution of the Eastern Mediterranean. This understanding takes on societal importance when it looks at the island's recent uplift history, as such inspection can provide indications for potential hazards related to seismicity, tsunamis and coastal change, which are natural phenomena associated with crustal uplift.

Uplift of MIS-3 and 4 deposits

Our data indicate that sediments of the Kashanes gravel and Kiti Tower sand, which today are at elevations as high as 30 m above SL, were deposited during MIS-3 and 4, a period covering much of the Earth's last glacial interval. Eustatic SL during this period was well below that of the present and for MIS-3, SL ranged from 40 to 90 m below that of today (Waelbroeck *et al.* 2002; Siddall *et al.* 2003, 2008; Lambeck & Purcell 2005; Shackleton *et al.* 2000). Based on those values, assuming that dated sediments were deposited near SL, and without taking into account any depth of water during deposition, outcrops of MIS-3 sediments at *c.* 30 m on the Larnaca Lowlands shelf are *c.* 70–120 m above the elevation expected for SL at that time (Fig. 8).

Dividing the data into age populations of *c.* 25–26 and *c.* 40 ka, which obtain maximum observed elevations of *c.* 12 and *c.* 30 m, respectively, our calculated uplift rate for the younger population is *c.* 2.1–4.1 mm/year and for the older population is *c.* 1.8–3.0 mm/year. These rates are much greater than previous uplift estimates of *c.* .05 mm/year

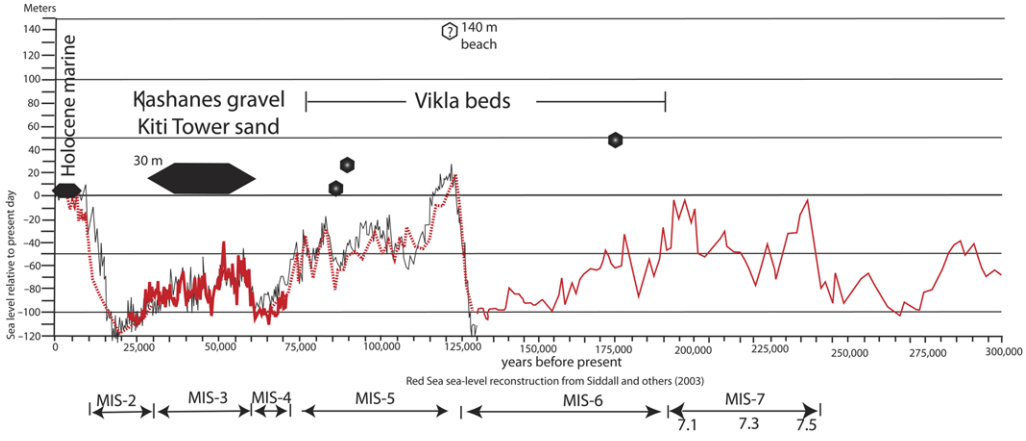

Fig. 8. Plot of marine geochronology v. age and sea-level curves; red line is reconstruction (±12 m) for Red Sea by Siddall *et al.* (2003), including high-resolution (±12 m) section for MIS3 interval. Black line is reconstruction curve from Shackleton *et al.* (2000) for Atlantic coast of Iberian Peninsula.

since the Late Pleistocene (Poole *et al.* 1990; Poole & Robertson 1991), but are similar to values determined by Vita-Finzi (1990) for western Cyprus. Our calculated rates would be greater if a depth of water column was added to the calculations.

The occurrence of MIS-3 and 4 deposits above present SL at Larnaca, Famagusta, Ayia Napa (GSD 2010) and western Cyprus (Vita-Finzi 1990) strongly suggests that at least the southern two-thirds of the island of Cyprus that are underlain by

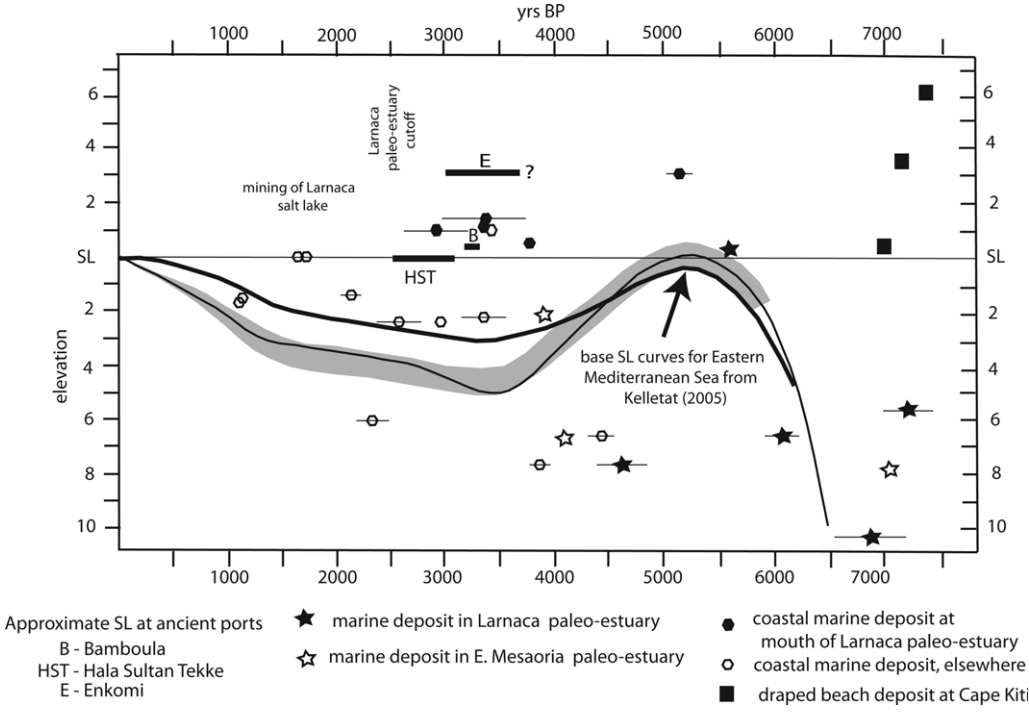

Fig. 9. Plot of Holocene age data and Holocene SL curves for Eastern Mediterranean from Kelletat (2005). The three SL curves shown by Kelletat vary owing to different sedimentological and geomorphological arguments.

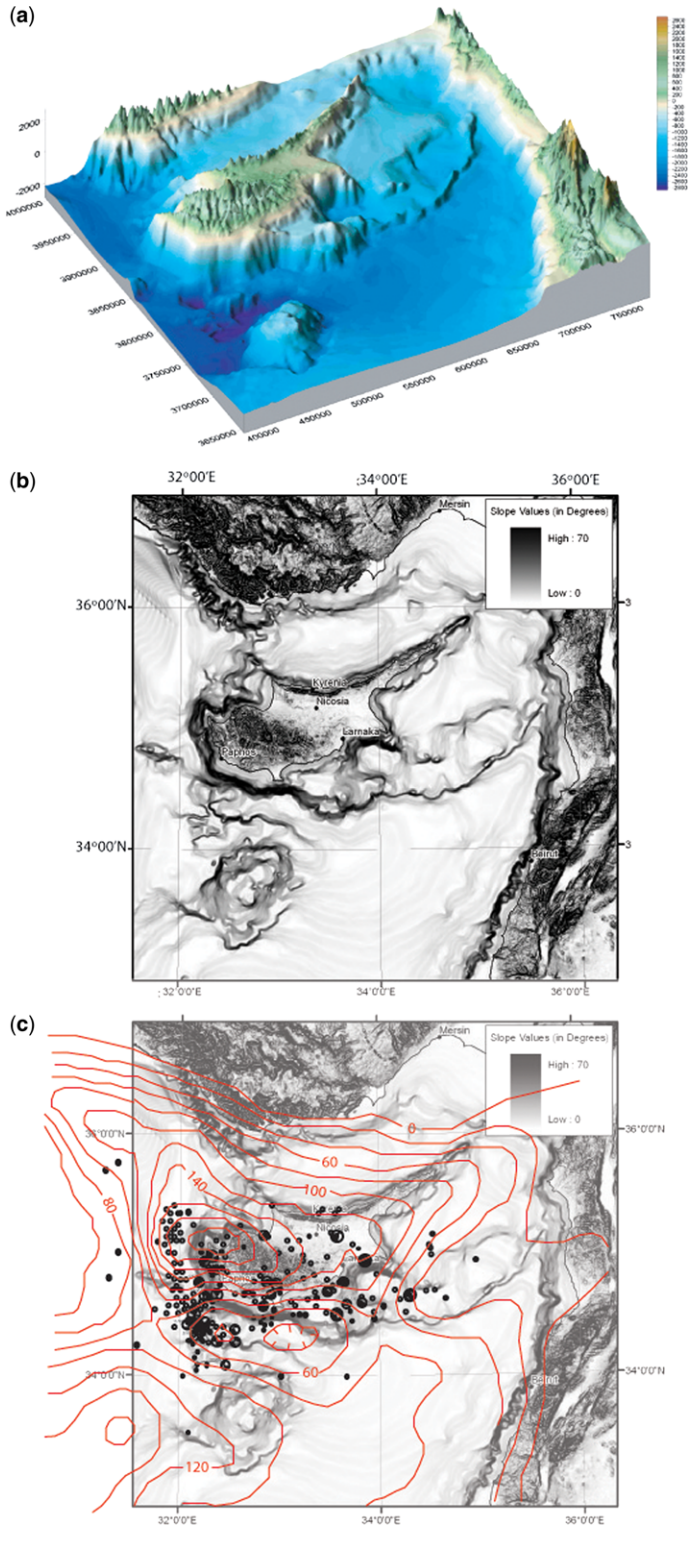

the Troodos Ophiolite have been uplifted uniformly since the latest Pleistocene. In terms of uplift, the Troodos Ophiolite appears to be behaving as a coherent structural block; a similar conclusion was drawn by Kinnaird *et al.* (2011) and McCallum & Robertson (1990).

Holocene uplift

A Holocene uplift rate can be estimated by comparing age and the elevation of the Holocene marine deposits with baseline Holocene SL curves of Kelletat (2005). The resulting plot (Fig. 9) shows that many deposits lie above the baseline curves, even though we are assuming no water column above our samples. This indicates that uplift has continued into Middle to Late Holocene times. This indication is in agreement with archaeological data from Hala Sultan Tekke (Åström *et al.* 1983) on the western side of the Main Salt Lake that suggest that SL during Late Bronze Age occupation was approximately at present SL; from the Phoenician harbour of Bamboula on the Mediterranean coast by Morhange *et al.* (2000), who report fossiliferous marine sediment at 40 cm above present SL; and tentatively from Enkomi, where stone ship moorings exist at *c.* 3–4 m above SL (Fig. 9). Using the elevations of samples 11/19/09-4, 5 and 6 collected from the mouth of the palaeo-estuary, which are *c.* 4–6 m above Holocene baseline curves and assuming no water column, an uplift rate of *c.* 1.2–2.1 mm/year is indicated. Using the elevations of *Posidonia oceanic* mats (samples 11/21/09–2 and 3), which are *c.* 2.0–3.5 m above baseline curves and assuming no water column, an uplift rate of *c.* 1.2–2.1 mm/year also is indicated. If indications of past SL at the archaeological sites are used, then uplift rates of *c.* 1.1–1.7 (Hala Sultan Tekke), *c.* 1.1–1.4 (Bamboula) and tentatively *c.* 2.0–2.7 mm/year (Enkomi) are suggested for Middle to Late Holocene time.

Mechanisms of uplift

The island of Cyprus is fundamentally the massif of the Troodos Ophiolite. McCallum & Robertson (1990) concluded that the Troodos Ophiolite has experienced pulsed uplift in the Miocene, Pliocene and Pleistocene. Kinnaird *et al.* (2011) concluded that relatively high rates of uplift of the Troodos Ophiolite persisted into Middle and Late Pleistocene time. This study demonstrates that uplift continued into the Late Pleistocene and Holocene. Our recognition of an island-wide uplift rate that is of orogenic magnitude leads to an important question on plate-margin tectonic processes: what mechanism drives this uplift?

We can envisage three broad categories of processes that could generate uplift: lithospheric response to glacial (climatic-driven) processes, diapirism from serpentinization of mantle rocks and tectonic crustal deformation. We cannot rule out some uplift from glacial processes, but addressing that is beyond the scope of this paper. Localized diapirism and uplift are occurring at Mt Olympus in the Troodos Mountains owing to serpentinization of the Troodos Ophiolite, but it is difficult to imagine this process as affecting the entire massif, particularly given the gravity anomaly beneath Cyprus (Harrison 1955). Therefore, we will consider only tectonic processes for uplift of Cyprus.

We view areas of high relief and steep slope on the Earth's surface as indicators of where active uplift is occurring. Looking at crustal relief and slope in the Cyprus region (Fig. 10a, b), our conclusion is that uplift is occurring in narrow zones along the coasts or nearby offshore. These zones trend dominantly NNW, NNE and east–west ($\pm 20^{\circ}$), similar to those of structural trends found in the Troodos Ophiolite. It is our opinion that the zones of steep slope shown in Figure 10b correspond to fault zones that are reactivated Troodos structures.

Three fault zones (FZ) contribute to uplift of SE Cyprus (Fig. 11): NNW-trending Famagusta FZ, east–west-trending Latakia FZ and NNE-trending Larnaca FZ. Our mapping of the onshore portion of the Famagusta FZ found it to consist of parallel eastward-dipping, high-angle reverse faults. The westernmost strand, Enkomi fault, is expressed at the surface as a monoclinal fold that has uplifted Kiti Tower sand *c.* 10–15 m; fracture-fill yielded an OSL age of 5.4 $\pm$ 2.3 ka (Table 2), indicating that this fault has a Holocene history. The Latakia FZ and the Larnaca FZ form two sides of the Cyprus Basin, which is a Neogene pull-apart graben (Vidal *et al.* 2000; Harrison *et al.* 2010) – an area of transtension created by a left-step in a left-lateral, strike-slip system. The floor of the basin is only slightly deeper than the seafloor to the east (Fig. 10a), indicating that, rather than the basin subsiding, Cyprus is being uplifted around the area of transtension. Marine seismic data (Vidal *et al.* 2000) show the Latakia FZ to be a left-lateral, positive-flower structure with steeply dipping transpressive faults, consistent with focal-mechanism

Fig. 10. (**a**) Oblique view of coloured DEM of the Cyprus. (**b**) Plan view of slope (first derivative) of Earth's surface in the Cyprus region. (**c**) Overlay of Bouguer gravity contours from Ergün *et al.* (2005), and earthquake epicentres from Papadimitriou & Karakostas (2006) and Pinar & Kalafat (1999).

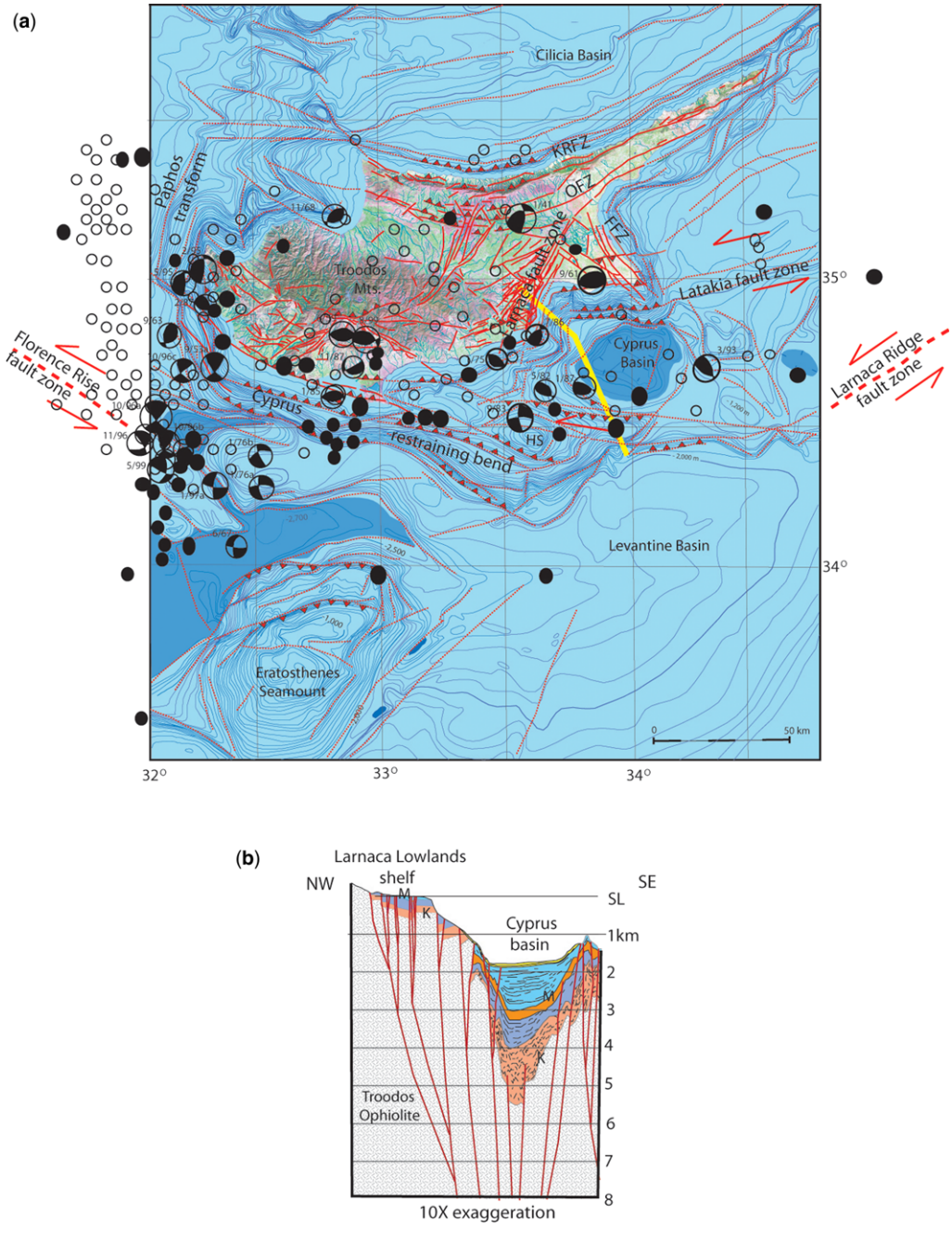

Fig. 11. (**a**) Map of neotectonic faults on and surrounding Cyprus. Onshore faults are from reconnaissance mapping by authors, Harrison *et al.* (2008), and GEOTER (2005). Offshore faults are interpreted from sea-floor relief and linear features. Beach-ball symbols show focal mechanisms for events M > 5.5 (dark areas are compressional quadrants) and filled-black circles are events >M4 for the period 1940–1992 from Salamon *et al.* (2003); open circles are epicentres after Pinar & Kalafat (1999) for the period April 1997 to January 1998. KRFZ, Kyrenia Range fault zone; OFZ, Ovgos fault zone; FFZ, Famagusta fault zone; HS, Herodotus Seamount. Yellow line is line of cross section. (**b**) Cross section from Larnaca Lowlands through the Cyprus Basin; onshore portion is from this report, offshore portion is after Vidal *et al.* (2000). M is the Messinian reflector; K is top of Cretaceous reflector from Vidal *et al.* (2000).

analyses (Papadimitriou & Karakostas 2006). The Larnaca FZ consists of braided faults that extend onshore for >35 km (Harrison & Tsiolakis 2007) and is part of a wider system of faults that accommodate displacement into the Cyprus Basin (Fig. 11b). Restraining bends along the Larnaca FZ have produced localized uplift, such as at Cape Kiti, where a draped beach-gravel has been uplifted *c.* 6.5 m. Two bivalves from this deposit yielded ^{14}C ages of 7083 ± 100 and 7454 ± 67 cal-year-bp. These values plot well above the steep section of the Holocene SL curves (Fig. 9); thus direct estimates of uplift rate are not feasible. However, indirectly, estimates of a Holocene uplift at Cape Kiti are possible by comparison with elevations of similar-aged deposits. Gifford (1978) collected *Posidonia oceanica* fibres from two holes drilled into the Larnaca Salt Lakes estuary (west of the Larnaca FZ) at elevations of 5.5 and 10.8 m below SL. Our calibration of his reported ^{14}C ages are 7217 ± 267 and 6908 ± 404 cal-year-bp, which are similar to ages of the Cape Kiti draped beach gravel. Relative to Gifford's (1978) estuarine deposits and assuming *c.* 2 m of water column, the draped beach gravel at Cape Kiti has been uplifted *c.* 10–15 m. These values suggest *c.* 1.4–2.0 mm/year of uplift at Cape Kiti over our estimate of regional Holocene uplift. This difference can be considered an approximate proxy for Holocene fault-slip rate along the Larnaca FZ there. On the north side of Larnaca, drill-hole and geophysical data indicate *c.* 45 m of post-Pliocene uplift across the Larnaca FZ and *c.* 2–3 m of uplift on the base of the Holocene marine section (Harrison & Tsiolakis 2007). Also, we attribute the closure of the Larnaca Salt Lakes palaeo-estuary at *c.* 2.5 ka to coastal uplift of *c.* 2–3 m owing to localized transpression and uplift along the Larnaca FZ. Earthquake-focal-mechanism resolutions along the western margin of the Cyprus Basin (Salamon *et al.* 2003) are consistent with fault orientations and kinematics determined for the Larnaca FZ (Fig. 11a).

On the south side of Cyprus, zones of high-relief and slope occur dominantly offshore and trend WNW (Fig. 10a, b) along what we consider a restraining-bend section of the Cyprus transform (Harrison *et al.* 2004, 2008) at the Anatolian–African plate boundary (Fig. 11). Focal mechanisms (Fig. 11a) are left-lateral and transpressive (Salamon *et al.* 2003), consistent with positive-flower-structures imaged by marine geophysics (Vidal *et al.* 2000). The only onshore expression along this structural trend is in the Paphos area, where north-dipping, high-angle thrusts faults have been mapped by GEOTER (2005). On the west side of Cyprus, high-relief and slope occur offshore along the northerly trending Paphos transform zone of Papazachos & Papaioannou (1999). Focal-mechanism resolutions there (Fig. 11a) are right-lateral strike-slip and transpressive along east-dipping surfaces (Papadimitriou & Karakostas 2006). The downward projections of the high-relief and slope gradients to seismogenic depths off the west coast of Cyprus closely coincide with concentrations of seismicity (Fig. 11c). A concave-northward, curved zone of high relief and slope occurs immediately offshore on the north coast of Cyprus (Fig. 10a, b); presumably, this is related to the Kyrenia Range thrust system.

We are impressed by spatial relationships and similarity of trends between the linear zones of high relief, seismicity and gravity gradients associated with the Troodos Ophiolite. It is our opinion that these phenomena and the uniform, island-wide Late Pleistocene–Holocene uplift are results of the western movement of the Troodos Ophiolite, which is driven by the escape tectonics of the Anatolian microplate (Fig. 1). We further believe that this movement is probably accommodated by slippage along pre-existing detachment fabric at the base of the ophiolite massif and underlying metamorphic–sole structural fabric.

Gass & Masson-Smith (1963) determined from geophysical analysis that the base of the Troodos Ophiolite beneath Cyprus is a low-angle northward-dipping surface (Fig. 12a, b). A geophysical survey of the Eastern Mediterranean by Aal *et al.* (2001) shows a similar low-angle structure at the base of the Troodos Ophiolite, which overlies continental crust in their lithospheric cross section. There are other low-angle, northward-dipping structures of regional significance (Figs 1 & 12c) known to exist in northern Cyprus, such as the Ovgos FZ (Harrison *et al.* 2004, 2008) and the Kyrenia Range FZ (Robertson 2000; Harrison *et al.* 2004, 2008); and both structural zones have accommodated contraction during the Neogene (Robertson, 2000; Harrison *et al.* 2004, 2008). As first noted by Kempler & Garfunkel (1994), the Cilicia Basin north of Cyprus is not affected by regional compression, indicating that compression/transpression along the Anatolian plate boundary is absorbed with Cyprus, which is fundamentally the Troodos ophiolite.

We suggest the possibility that, accompanying neotectonic deformation along the margins of the Troodos ophiolite, the low-angle detachment fault at the base of the Troodos also has been active during the Neogene (Fig. 12c). In this hypothesis, which is similar to a proposal by McCallum & Robertson (1990) that called for under-thrusting from the south of a continental crustal block beneath Cyprus, re-activation of the basal detachment fault has contributed to partitioning of strain and uplift of the Troodos Ophiolite in the form of a tectonic wedge. This model is similar to that described by

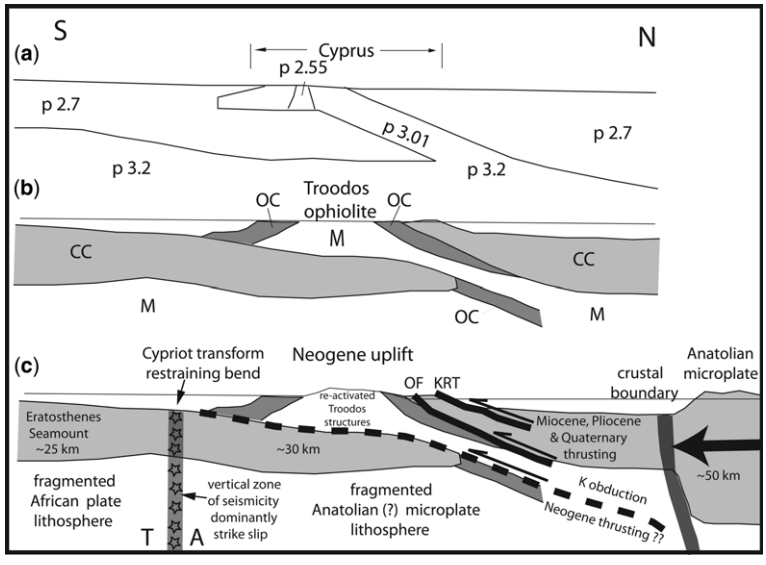

Fig. 12. North–south crustal cross sections through Cyprus. (**a**) Model of gravity data showing rock densities after Gass and Mason-Smith (1963). (**b**) Interpretation of crustal material by Gass and Mason-Smith (1963): CC, continental crust; OC, oceanic crust; M, mantle material. (**c**) Above section showing the location of seismicity along the Cypriot transform, area of Neogene uplift along the margins of the Troodos Ophiolite, and our interpretations of north-dipping structures that accommodate lithospheric contraction. KRT, Kyrenia Range thrust system (Neogene); OF, Ovgos fault zone (Neogene and Palaeogene); T, towards; A, away.

Langenheim *et al.* (2005) and Graymer *et al.* (2007) for tectonic wedging along a restraining bend along the San Andreas fault zone. We envisage this tectonic wedge as being driven south and southwestward over continental crust that is restrained from southward movement by the Cyprus-restraining-bend section of the transform plate boundary. Such a suggestion has strong implications for seismic and tsunami hazards and warrants further investigated.

We thank the Fulbright Commission and Office of Foreign Disaster Assistance of the US State Department for funding to conduct the majority of this research. We also thank M. Pavich, T. Cronin, C. Fita-Finzi, A. H. F. Robertson, T. Kinnaird, and an anonymous reviewer for comments and suggestions that improved the science and clarity of this manuscript.

References

Aal, A., Barkooky, A., Gerrits, M., Meyer, H., Schwander, M. & Zaki, H. 2001. Tectonic evolution of the eastern Mediterranean Basin and its significance for the hydrocarbon prospectivity of the Nile Delta deepwater area. *GeoArabia*, **6**, 363–384.

Åström, P., Åström, E., Hatziantoniou, A., Niklasson, K. & Öbrink, U. 1983. *Hala Sultan Tekke 8, Excavations 1971–1979*. Studies in Mediterranean Archaeology XLV:8. Paul Åströms Förlag, Typografia, Göteborg.

Bagnall, P. S. 1960. *The Geology and Mineral Resources of the Pano Lefkara–Larnaca Area*. Geological Survey Department of Cyprus, Nicosia, Memoirs, **5**.

Bridwell, R. J. 1975. Sinuosity of strike-slip fault traces. *Geology*, **3**, 630–632.

Burke, K. & Şengör, A. M. C . 1986. Tectonic escape in the evolution of the continental crust. *In*: Barazangi, M. & Brown, L. D. (eds) *Reflection Seismology: The Continental Crust*. American Geophysical Union, Washington, DC, Geodynamics Series, **14**, 41–53.

Devillers, B., Morhange, C., Buffière de l'Air, M. & Provansal, M. 2002. Détritisme potentialities et aménagements du territoire à l'age du bronze. *Ahier du Centre d'Études Chypriotes*, **32**, 33–52.

Dewey, J. F., Pitman, W. C., Ryan, W. B. F. & Bonnin, J. 1973. Plate tectonics and the evolution of the Alpine system. *Bulletin of the Geological Society of America*, **84**, 3137–3180.

Eaton, S. 1987. *The Sedimentology of Mid to Late Miocene carbonates and evaporites in southern Cyprus*. PhD thesis, University of Edinburgh.

Ergün, M.,, Okay, S., Sari, C., Oral, E. Z., Ash, M., Hall, J. & Miller, H. 2005. Gravity anomalies of the Cyprus Arc and their tectonic implications. *Marine Geology*, **221**, 349–358.

Gajarda, E. & Makris, J . 1998. *Seismic Hazard and Design Conditions for the New International Airport of Larnaca, Cyprus*. Geological Survey Department of Cyprus, Nicosia.

GARFUNKEL, Z. 1998. Constraints on the origin and history of the eastern Mediterranean basin. *Tectonophysics*, **29**, 5–35.

GASS, I. & MASSON-SMITH, D. 1963. The geology and gravity anomalies of the Troodos Massif, Cyprus. *Philosophical Transactions of the Royal Society of London*, **255**, 417–467.

GAUDRY, A. 1862. Géologie de l'ile de Chypre. *Memoirs of the Society of Geologists of France*, **2**, 149–307.

GEOLOGICAL SURVEY DEPARTMENT, CYPRUS. 2010. Study of the geomorphology of Cyprus. Unpublished report by Metakron Consortium, Geological Survey Department of Cyprus, Nicosia.

GEOTER. 2005. *Study of Active Tectonics in Cyprus for Seismic Risk Mitigation*. Geological Survey Department of Cyprus, Nicosia.

GIFFORD, J. A. 1978. *Paleogeography of archaeological sites of the Larnaca Lowlands, southeastern Cyprus*. PhD thesis, University of Minnesota.

GOODFRIEND, G. A. 1987. Radiocarbon age anomalies in shell carbonate of land snails from semi-arid areas. *Radiocarbon*, **29**, 159–167.

GRAYMER, R. W., LANGENHEIM, V. E., SIMPSON, R. W., JACHENS, R. C. & PONCE, D. A. 2007. Relatively simple through-going fault planes at large-earthquake depth may be concealed by surface complexity of strike-slip faults. *In*: CUNNINGHAM, W. D. & MANN, P. (eds) *Tectonics of Strike-Slip Restraining and Releasing Bends*. Geological Society, London, Special Publications, **290**, 189–201.

HARRISON, J. C. 1955. An interpretation of the gravity anomalies of the eastern Mediterranean. *Philosophical Translations of the Royal Society of London Series A*, **248**, 283–325.

HARRISON, R. & PANAYIDES, I . 2004. A restraining-bend model for the tectonic setting and uplift of Cyprus. *In*: CHATZIPETROS, A. A. & PAVLIDES, S. B. (eds) *5th International Symposium on Eastern Mediterranean Geology*, Thessalonili, 14–20 April, 2004, B43–B46.

HARRISON, R. W. & TSIOLAKIS, E. 2007. Late Pleistocene and Holocene deformation along the Larnaca fault zone, Cyprus. (Abstract.) *In*: *6th International Symposium of Eastern Mediterranean Geology Abstracts Volume*, 2–5 April, Amman, 18.

HARRISON, R., NEWELL, W. *ET AL*. 2004. Tectonic framework and late Cenozoic tectonic history of the northern part of Cyprus: implications for earthquake hazards and regional tectonics. *Journal of Asian Earth Sciences*, **23**, 191–210.

HARRISON, R. W., NEWELL, W. *ET AL*. 2008. *Bedrock geologic map of the greater Lefkosia area, Cyprus*. US Geological Survey Scientific Investigations Map, **3046**.

HARRISON, R. W., TSIOLAKIS, E., STONE, B. D., LORD, A. R., MAHAN, S. A. & MCGEEHIN, J. P . 2010. The role of Late Pleistocene-Holocene faulting in the Larnaca Lowlands, Cyprus in the pull-apart growth of the Cyprus Basin and implications for active tectonics along the African-Anatolian plate boundary. (Abstract.) *In*: *7th International Symposium on Eastern Mediterranean Geology Abstract Book*, 18–22 October, 2010, Adana, Turkey, **31**.

JACKSON, J. & MCKENZIE, D. 1988. The relationship between plate motions and seismic moment tensors, and the rates of active deformation in the Mediterranean and Middle East. *Geophysical Journal*, **93**, 45–73.

KELLETAT, D. 2005. A Holocene sea level curve for the eastern Mediterranean from multiple indicators. *Annals of Geomorphology*, **137**, 1–9.

KEMPLER, D. & GARFUNKEL, Z. 1994. Structures and kinematics in the northeastern Mediterranean: A study of an irregular plate boundary. *Tectonophysics*, **234**, 19–32.

KINNAIRD, T. C., ROBERTSON, A. H. F. & MORRIS, A. 2011. Timing of uplift of the Troodos Massif (Cyprus) constrained by sedimentary and magnetic polarity evidence. *Journal of the Geological Society*, **168**, 457–470.

LAMBECK, K. & PURCELL, A. 2005. Sea-level change in the Mediterranean Sea since the LGM: model predictions for tectonically stable areas. *Quaternary Science Reviews*, **24**, 1969–1988.

LANGENHEIM, V. E., JACHENS, R. C., MATTI, J. C., HAUKSSON, E., MORTON, D. M. & CHRISTENSEN, A. 2005. Geophysical evidence for wedging in the San Gorgonio Pass structural knot, southern San Andreas fault zone, southern California. *Geological Society of America Bulletin*, **117**, 1554–1572.

MAHMOUD, S., REILINGER, R., MCCLUSKY, S., VERNANT, P. & TEALEB, A. 2005. GPS evidence for northward motion of the Sinai Block: implications for E. Mediterranean tectonics. *Earth and Planetary Science Letters*, **238**, 217–224.

MAKRIS, J., STACKER, J. & KRAMVIS, S. 2000. Microseismic studies and tectonic implications of Cyprus. *In*: PANAYIDES, I., XENOPHONTOS, C. & MALPAS, J. (eds) *Proceedings of the Third International Conference on the Geology of the Eastern Mediterranean*. Geological Survey Department of Cyprus, Nicosia, 137–145.

MANN, P. 2007. Global catalogue, classification and tectonic origins of restraining- and releasing bends on active and ancient strike-slip fault systems. *In*: CUNNINGHAM, W. D. & MANN, P. (eds) *Tectonics of Strike-Slip Restraining and Releasing Bends*. Geological Society, London, Special Publications, **290**, 13–142.

MCCALLUM, J. E. 1989. *Sedimentation and tectonics of the Plio-Pleistocene of Cyprus*. PhD thesis, University of Edinburgh.

MCCALLUN, J. E. & ROBERTSON, A. H. F. 1990. Pulsed uplift of the Troodos Massif-Evidence from the Plio-Pleistocene Mesaoria Basin. *In*: MALPAS, J., MOORES, E. M., PANAYIOTOU, A. & XENOPHONTOS, C. (eds) *Ophiolites, Oceanic Crustal Analogues: Proceedings of the symposium 'Troodos 1987'*. Geological Survey Department of Cyprus, Nicosia, 217–230.

MCCLUSKY, S., BALASSANIAN, S. *ET AL*. 2000. Global positioning system constraints on plate kinematics and dynamics in the eastern Mediterranean and Caucasus. *Journal of Geophysical Research*, **105**, 5,695–5,719.

MCKENZIE, D. P. 1970. Plate tectonics of the Mediterranean region. *Nature*, **220**, 239–343.

MORHANGE, C., GOIRAN, J.-P. *ET AL*. 2000. Recent Holocene paleo-environmental evolution and coastline

changes of Kition, Larnaca, Cyprus, Mediterranean Sea. *Marine Geology*, **170**, 205–230.

NEEV, D. 1977. The Pelusium Line-A major transcontinental shear. *Tectonophysics*, **38**, 1–8.

PAPADIMITRIOU, E. E. & KARAKOSTAS, V. G. 2006. Earthquake generation in Cyprus revealed by the evolving stress field. *Tectonophysics*, **423**, 61–72.

PAPAZACHOS, B. C. & PAPAIOANNOU, C. A. 1999. Lithospheric boundaries and plate motions in the Cyprus area. *Tectonophysics*, **308**, 193–204.

PINAR, A. & KALAFAT, D. 1999. Source process and seismotectonic implications of the 1995 and 1996 Cyprus, Eastern Mediterranean region, earthquakes. *Tectonics*, **301**, 217–230.

POOLE, A. J. & ROBERTSON, A. H. F. 1991. Quaternary uplift and sea-level change at an active plate boundary, Cyprus. *Journal of the Geological Society of London*, **148**, 909–921.

POOLE, A. J., SHIMMIELD, G. B. & ROBERTSON, A. H. F. 1990. Late Quaternary uplift of the Troodos ophiolite, Cyprus: uranium-series dating of Pleistocene coral. *Geology*, **18**, 894–897.

PRESCOTT, J. R. & HUTTON, J. T. 1994. Cosmic ray contribution to dose rates for luminescence and ESR dating: large depths and long-term time variations. *Radiation Measurements*, **23**, 497–500.

REIMER, P. J., BAILLIE, M. G. L. *ET AL.* 2009. INTCAL09 and MARINE09 radiocarbon age calibration curves, 0–50 000 years cal bp. *Radiocarbon*, **51**, 1111–1150.

ROBERTSON, A. H. F. 1977. Tertiary uplift of the Troodos Massif, Cyprus. *Geological Society of America Bulletin*, **88**, 1763–1772.

ROBERTSON, A. H. F. 2000. Tectonic evolution of Cyprus in its easternmost Mediterranean setting. *In*: PANAYIDES, I., XENOPHONTOS, C. & MALPAS, J. (eds) *3rd International Conference on the Geology of the Eastern Mediterranean*. Geological Survey Department of Cyprus, Nicosia, 11–44.

ROBERTSON, A. H. F., KIDD, R. B. *ET AL.* 1995. Eratosthenes Seamount: collisional processes in the easternmost Mediterranean in relation to Plio-Quaternary uplift of southern Cyprus. *Terra Nova*, **7**, 254–264.

SALAMON, A., HOFSTETTER, A., GARFUNKEL, Z. & RON, H. 2003. Seismotectonics of the Sinai subplate – the eastern Mediterranean region. *Geophysical Journal International*, **155**, 149–173.

SCHATTNER, U. 2010. What triggered the early-to-mid Pleistocene tectonic transition across the entire eastern Mediterranean? *Earth and Planetary Science Letters*, **289**, 539–548.

ŞENGÖR, A. M. C., GORUR, N. & SAROGLU, F. 1985. Strike-slip faulting and related basin formation in zones of tectonic escape: Turkey as a case study. *In*: BIDDLE, K. T. & CHRISTIE-BLICK, N. (eds) *Strike-Slip Deformation, Basin Formation, and Sedimentation*. Society of Economic Paleontologists and Mineralogists, Special Publications, **37**, 227–264.

SHACKLETON, N. J., HALL, M. A. & VINCENT, E. 2000. Phase relationships between millennial-scale events 64 000–24 000 years ago. *Paleoceanography*, **15**, 565–569.

SIDDALL, M., ROHLING, E. J., ALMOGI-LABIN, A., HEMLEBEN, Ch., MEISCHNER, D., SCHMELZER, I. & SMEED, D. A. 2003. Sea-level fluctuations during the last glacial cycle. *Nature*, **423**, 853–858.

SIDDALL, M., ROHLING, E. J., THOMPSON, W. G. & WAELBROECK, C. 2008. Marine isotope stage 3 sea level fluctuations: Data synthesis and new outlook. *Reviews of Geophysics*, **46**, RG4003.

STOW, D. A. V., BRAAKENBURG, N. E. & XENOPHONTOS, C. 1995. The Pissoui Basin fan-delta complex, southwestern Cyprus. *Sedimentary Geology*, **98**, 245–262.

STUIVER, M. & REIMER, P. J. 1993. Extended C-14 database and revised Calib 3.0 C-14 age calibration program. *Radiocarbon*, **35**, 215–230.

SWANSON, M. T. 2005. Geometry and kinematics of adhesive wear in brittle strike-slip fault zones. *Journal of Structural Geology*, **27**, 871–887.

TEN VEEN, J. H., WOODSIDE, J. M., ZITTER, T. A. C., DUMONT, J. F., MASCLE, J. & VOLKONSKAIA, A. 2004. Neotectonic evolution of the Hellenic and Cyprus arcs. *Tectonophysics*, **391**, 35–65.

TRUMBORE, S. E. 2000. Radiocarbon geochronology. *In*: NOLLER, J. S., SOWERS, J. M. & LETTIS, W. R. (eds) *Quaternary Geochronology*. American Geophysical Union, Washington, DC, 41–60.

VIDAL, N., ALVAREZ-MARRON, J. & KLAESCHEN, D. 2000. The structure of the Africa-Anatolia plate boundary in the eastern Mediterranean. *Tectonics*, **19**, 723–739.

VITA-FINZI, C. 1990. ^{14}C dating of Late Quaternary uplift in western Cyprus. *Tectonophysics*, **172**, 135–140.

WAELBROECK, C. L., LABEYRIE, L. *ET AL.* 2002. Sea-level and deep water temperature changes derived from benthic foraminifera isotopic records. *Quaternary Science Reviews*, **21**, 295–305.

WDOWINSKI, S., BEN-AVRAHAM, Z., ARVIDSSON, R. & EKSTRÖM, G. 2006. Seismotectonics of the Cyprian arc. *Geophysical Journal International*, **164**, 176–181.

WOODSIDE, J. M. 1977. Tectonic elements and crust of the eastern Mediterranean Sea. *Marine Geophysical Research*, **3**, 317–354.

YON, M. 1994. Kition-Bamboula: *In:* CHRISTOU, D. (ed.) *Chronique des fouilles et découvertes archéologiques á Chypre en 1993.*. Bulletin de Correspondance Hellénique, **118**, 672–677.